

Entangling gates for trapped-ion quantum computation and quantum simulation

Zhengyang Cai,¹ Chunyang-Luan,¹ Lingfeng Ou,¹ Hengchao Tu,¹ Zihan Yin,¹ Jing-Ning Zhang,² and Kihwan Kim^{1, 2, 3, 4, *}

¹*State Key Laboratory of Low Dimensional Quantum Physics, Department of Physics, Tsinghua University, Beijing 100084, China*

²*Beijing Academy of Quantum Information Sciences, Beijing 100193, China*

³*Hefei National Laboratory, Hefei 230088, P. R. China*

⁴*Frontier Science Center for Quantum Information, Beijing 100084, China*

The trapped-ion system has been a leading platform for practical quantum computation and quantum simulation since the first scheme of a quantum gate was proposed by Cirac and Zoller in 1995. Quantum gates with trapped ions have shown the highest fidelity among all physical platforms. Recently, sophisticated schemes of quantum gates such as amplitude, phase, frequency modulation, or multi-frequency application, have been developed to make the gates fast, robust to many types of imperfections, and applicable to multiple qubits. Here, we review the basic principle and recent development of quantum gates with trapped ions.

I. INTRODUCTION

In 1995, the first quantum gate for quantum computation was proposed and realized with trapped ions [1–3]. Since the proposal by Cirac and Zoller [1], the trapped ion system has led the field of quantum computation [4–8] as well as quantum simulation [9]. The Cirac-Zoller (CZ) gate is based on specifically using the center of mass vibrational mode. The CZ gate requires perfect ground-state cooling and individual addressing on the target ions, which makes it difficult to be a high-fidelity gate. In 1999, Mølmer and Sørensen proposed a different type of entangling gate, which relaxes the requirements of perfect ground state cooling and individual addressing, and the gates were realized with up to four qubits by NIST group [10–13]. Almost at the same time, a gate using geometric phase in the vibrational mode space from conditional displacement operation was proposed and realized with decent fidelity [14–16], which was also named as light-shift (LS) gate. It has a similar level of experimental requirements to the Mølmer-Sørensen (MS) gate. Later, the MS gate was understood in terms of the geometric phase in the phase space of position and momentum, which unifies the understanding of the MS gate and LS gate [12, 17].

Basically, both the LS [16] and the MS gates can be understood as the specific usage of a force dependent on a qubit state. For the LS gate [16], the force is dependent on the ion-qubit state in the σ_z basis, and for the MS gate, it is dependent on the ion-qubit state in the σ_ϕ -basis, where $\sigma_\phi = \cos \phi \sigma_x + \sin \phi \sigma_y$ [12, 17]. Therefore, the LS gate and the MS gate are called σ_z - and σ_ϕ -gate, respectively. The LS and the MS gate have been improved and shown the fidelities of over 99.9 %, which have been the highest fidelities so far among all physical platforms for quantum computation [18–20].

One of the promising schemes to scale up the size of the ion-trap system is to entangle a small number of ion-qubits by using the LS or the MS gate in a single

zone and to connect different trapping zones by individually shuttling ions [21, 22], which is called a quantum charge-coupled device (QCCD) architecture. These entangling gates are typically realized by single or Raman laser beams with non-vanishing wave-vector \mathbf{k} . The laser implementations of the trapped-ion quantum gates have been successful with a small number of ion-qubits with high fidelities [18–20]. However, it could be challenging to apply numerous laser beams to different trapping zones for large-scale quantum computation based on the QCCD approach. The microwave or RF implementation could provide an alternative solution for implementing quantum gates on multiple zones since microwave or RF circuits can be integrated with the trap [23, 24]. These laser-less gates require a significant field gradient to couple qubits and vibrational modes. Two main methods have been explored in this direction; one is using static-magnetic-field gradient combined with microwave [25–28], and the other one is using oscillating-magnetic-field gradient at near-qubit frequency [23, 24, 29]. Recently, the third scheme has been implemented, which combines a near-motion-frequency field gradient and near-qubit-frequency field [30–32].

Alternatively, it has been proposed and realized to perform entangling gates on any two qubits in a large number of ions in a single trap zone, where the total number of vibrational modes increases with the number of ions in the zone [33–37]. In this case, it is necessary to take into account the effect of many collective vibrational modes, which is to disentangle target qubits and all relevant vibrational modes at the end of the gate. Originally, these requirements were proposed to be fulfilled by using amplitude modulation [33–35, 38]. Later, other methods such as phase [39–41] or frequency modulation [42–44], and multi-tone modulation [45–48], have been introduced for the purpose and others such as robustness or noise-resilience of the pairwise gates [45]. Moreover, these sophisticated methods of quantum gates can be also applied to make two-qubit gates without the speed limit [38].

Furthermore, these schemes were extended to simultaneously or parallelly entangle more qubits [48–51].

In this article, we provide the basic principle of quantum entangling gates with trapped ions and review the recent development of gates with sophisticated pulse modulations for various purposes. We point out that among many different types of modulations, the multi-frequency method captures the general control that covers all other modulation methods and provides systematic ways of optimizing the gates according to the purposes. Finally, we summarize some applications of the multi-frequency method for various purposes. This review article consists of the following sections. In section II, we introduce the basics of the trapped-ion system, such as different types of qubits, cooling, qubit initialization, detection, and single-qubit operations. In section III, we discuss the interactions between a two-level system coupled to a single vibrational mode, entangling gate operations with and without laser beams based on the qubit-state dependent force. In section IV, we summarize the modulation methods such as amplitude, phase, frequency, and multi-frequency, and show that the multi-frequency method has the most general aspect of control. In section V, we provide a general theoretical framework and examples of the multi-frequency method with or without individual controls to speed up the gate, make the gate robust against various noises and apply the gate on more than two ions simultaneously. Finally, we conclude the review article with an outlook.

II. BASICS OF THE TRAPPED-ION SYSTEM

Types of ion qubits

Served as a qubit, two internal levels of a trapped atomic ion are typically encoded as $|0\rangle$ and $|1\rangle$. Different from other artificial qubits, ion qubits are fundamentally identical, which is an advantageous feature for large-scale system development. The ion qubits have more unique advantages over other qubits in different physical platforms, such as the ultra-long coherence time up to the order of hours [52–55] and near-perfect qubit-state initialization and detection [53, 56, 57]. There are typically three types of qubits, where the energy splitting covers the frequency range of a few to tens of megahertz, gigahertz, and hundreds of terahertz, which correspond to the Zeeman qubit (Fig. 1(a)) [58], the hyperfine qubit (Fig. 1(b)) [16, 19, 59–61] and the optical qubit (Fig. 1(c)), respectively.

The Zeeman qubit is composed of a pair of Zeeman energy levels as shown in Fig. 1(a), and they can be manipulated by applying the radio-frequency (RF) or Raman lasers with frequency difference in the order of MHz [58]. For the Zeeman qubit, Doppler cooling, sideband cooling, and state initialization can be simply implemented

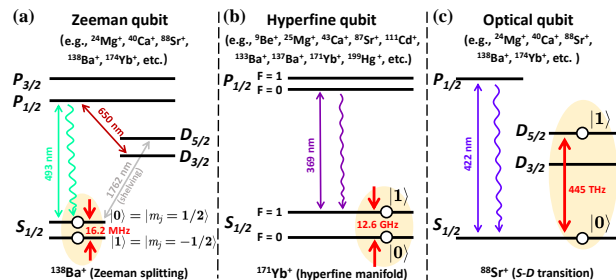


FIG. 1. The level structure of three typical types of ion-qubits (energy splittings not to scale). (a) The level splitting of Zeeman qubit is on the order of a few to tens of megahertz (as in $^{138}\text{Ba}^+$, etc.). (b) Hyperfine qubit, composed of a pair of ground-state hyperfine levels, has the level splitting on the order of a few to tens of gigahertz (as in $^{171}\text{Yb}^+$, etc.). (c) Consisting of one ground state and another metastable level, the optical qubit is driven by a light field on the order of a few hundred terahertz (as in $^{88}\text{Sr}^+$, etc.).

without any advanced experimental requirements such as high-frequency sidebands, narrow-line lasers, etc. However, the high-efficiency state discrimination of the Zeeman qubit requires another metastable energy level to shelve one of the qubit states. Moreover, the Zeeman qubit is sensitive to magnetic-field fluctuations, which results in a relatively short coherence time on the order of milliseconds. With the magnetic field shielding and permanent magnets, the coherence time of the Zeeman qubit has been increased to ~ 2.1 s with dynamical decoupling pulses [58]. For the optical qubit, one level in a ground state manifold and the other level in a metastable electronic state are used, which are typically separated by the electric quadrupole or octupole transition, as shown in the Fig. 1(c). The transitions can be driven with a single-frequency laser in the visible to near-IR spectrum region. Due to the long lifetime of metastable levels, the narrow-line laser (~ 1 Hz) stabilized by the high-finesse cavity is required to perform the optical transition. The coherence time of the optical qubit is similar to that of the Zeeman qubit. Technical efforts have been attempted to suppress phase fluctuations of the laser and push the coherence time to the ultimate limit of the upper-level decay [62].

Consisting of a pair of ground-state hyperfine levels, the hyperfine qubit can be driven by the microwave field [29, 63] or Raman lasers with the frequency difference in the order of GHz, as shown in Fig. 1(b). The hyperfine qubit can be implemented in “clock” transitions that are insensitive to the first-order magnetic field and have shown coherence time up to the order of hours [52–55]. Moreover, the dressed-states composed of ground-state hyperfine levels coupled with resonant RF field [26, 64] is an available qubit to realize a laser-less gate with a magnetic field gradient.

Cooling, state initialization, and detection

To obtain high-fidelity quantum entangling gates with trapped ions, motional-ground state cooling is necessary, which is realized by laser cooling methods. First, based on the velocity-dependent radiation force [65, 66], Doppler cooling can typically cool down ions to the order of millikelvin, which is limited by the natural linewidth of the cooled ions. Near ground-state cooling can be achieved by resolved-sideband cooling [67, 68]. Moreover, Sisyphus cooling [69, 70], or electromagnetically-induced-transparency (EIT) cooling provides an alternative to cooling a large number of modes of multiple ions simultaneously [71–78].

Before applying sequences of quantum gate operations, the ion qubits should be initialized to one of the qubit states. The state initialization is typically performed by the optical pumping technique within less than a few microseconds [79]. At the end of the quantum operations, the states of ion qubits can be measured via the state-dependent fluorescence detection [80, 81]. The ion qubit is projected to a bright state $|1\rangle$, which scatters lots of photons with the illumination of a detection laser, or a dark state $|0\rangle$ that scatters almost no photons. The scattered fluorescence photons are collected by an imaging system and detected by a photomultiplier tube (PMT) or charge-coupled device (CCD) typically. Recently, over 99.99 % detection fidelities have been demonstrated with optical qubits of $^{40}\text{Ca}^+$ and $^{138}\text{Ba}^+$ [56, 82]. For the hyperfine qubit of a single $^{133}\text{Ba}^+$ ion, around 99.97 % detection fidelity has been achieved [83]. For other hyperfine qubits with $^{43}\text{Ca}^+$ and $^{171}\text{Yb}^+$, over 99 % detection fidelities have been observed [56, 84]. The duration for the state detection typically takes around a few hundred μs to milliseconds. The shortest detection time was reported to $\sim 11 \mu\text{s}$ with 99.93 % average fidelity achieved by superconducting nanowire single-photon detectors (SNSPDs) [84].

Single-qubit operations

The single qubit operation can be driven by a resonant field to the qubit frequency, which can be realized by RF field [53], Raman lasers [19, 85] or the single laser [62]. The single qubit state is described as $|\psi\rangle = \cos(\theta/2)|0\rangle + e^{i\phi}\sin(\theta/2)|1\rangle$, where the Rabi frequency is $\Omega = \theta/t$, and it represents the coupling strength of field-matter interaction [4].

In the experiment, the highest fidelity of 99.9999 % single-qubit gates for the hyperfine qubit of $^{43}\text{Ca}^+$ has been performed by the near-field microwave [53]. With the Raman laser beams, the fidelities of over 99.99% have been demonstrated for the hyperfine qubits of $^{43}\text{Ca}^+$ and $^9\text{Be}^+$ [18, 19]. For optical qubits, over 99.99% fidelities of a single qubit gate have been achieved with a single

narrow-line laser [62].

In order to speed up the single-qubit gates, mainly technical efforts have been attempted. For the Raman method, the gate duration has been pushed to less than 50 ps [85, 86]. By using the microwave method, the gate with timescales of 20 ns has been performed [24]. In addition, the fidelity of ultra-fast single-qubit gate can be improved with the application of modulated pulse sequences and the suppression of unwanted excited transitions [87, 88].

For the single qubit operations with ion qubits, in particular, the hyperfine qubits, the main error sources are technical imperfections such as fluctuations in the amplitude of microwave fields. For the optical operations, the photon scattering from the relevant dipole transitions is an additional limiting factor [89], which makes lower fidelities than those of microwave gates. The coupling to vibrational modes in the single-qubit operations can be significantly suppressed by using fields with large wavelengths or copropagating-Raman schemes that nullify the coupling to vibrational modes. The coherence time of clock state qubits already reached over hours [52–55], which is not already a limiting factor for the fidelity of single-qubit operations.

III. A BRIEF EXPLANATION OF LASER AND LASERLESS GATES

Two-level system coupled to a single vibrational mode

For multi-qubit gates, quantum information stored in the internal states between trapped ions is transferred via coupling to the collective vibrational mode, the so-called “quantum bus”, which plays a core role in the quantum entangling gates [4, 5, 17]. With the near-resonant field, we just take into account a two-level system and one vibrational mode, and the general interaction Hamiltonian can be expressed as,

$$\hat{H}_{\text{int}} = \frac{\hbar}{2}\Omega[e^{i(kx-\omega t+\phi)} + e^{-i(kx-\omega t+\phi)}](\hat{\sigma}^+ + \hat{\sigma}^-), \quad (1)$$

where $\mathbf{k} \equiv k\hat{e}_x$, ω and ϕ are the wave vector, frequency, and phase of the field, respectively, $\Omega = \frac{|\mathbf{d}\cdot\mathbf{E}|}{\hbar}$ is the Rabi frequency, and $\hat{\sigma}^+ = |1\rangle\langle 0|$, $\hat{\sigma}^- = |0\rangle\langle 1|$. We assume the field is coupled to the vibrational mode in the x -radial direction. Transformed to the interaction picture with respect to $\hat{H}_0 = \frac{\hbar}{2}\omega_0\hat{\sigma}^z + \hbar\omega_m\hat{a}^\dagger\hat{a}$, the above interaction Hamiltonian (1) can be simplified after the rotating wave approximation (RWA),

$$\hat{H}'_{\text{int}} = \frac{\hbar}{2}\Omega\left\{\hat{\sigma}^+e^{i[\eta(\hat{a}^\dagger e^{i\omega_m t} + \hat{a}e^{-i\omega_m t} - \mu t + \phi)]}\right\} + \text{h.c.}, \quad (2)$$

where $\mu = \omega - \omega_0$ is the detuning between the field frequency and the qubit frequency ω_0 , ω_m is the motional

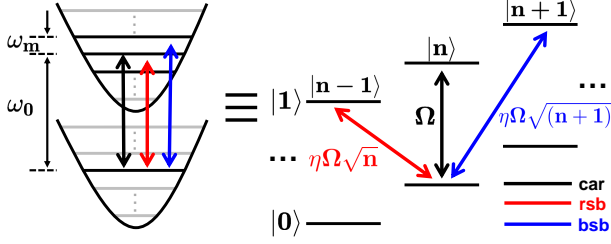


FIG. 2. The illustration for carrier and sideband transitions, where the ω_0 and ω_m are the qubit frequency and motional mode frequency. The abbreviations of car (black line), rsb (red line) and bsb (blue line) represent carrier, red- and blue-sideband transitions, respectively.

mode frequency, and $\eta = k\sqrt{\frac{\hbar}{2m\omega_m}}$ is the Lamb-Dicke parameter.

Generally, the phonon number $|n\rangle$ of trapped ions is cooled down to the Lamb-Dicke regime [4, 5, 17], where $\eta\sqrt{n+1} \ll 1$. And in this regime, the interaction Hamiltonian (2) can be further simplified to the following form,

$$\hat{H}_{LD} = \frac{\hbar}{2}\Omega\hat{\sigma}^+ [1 + i\eta(\hat{a}^\dagger e^{i\omega_m t} + \hat{a}e^{-i\omega_m t})] e^{i(\phi - \mu t)} + \text{h.c.} \quad (3)$$

In particular, we consider the three types of interaction, the carrier transition ($\mu = 0$), detuned blue ($\mu = \omega_m + \delta$), and red sideband transitions ($\mu = -\omega_m - \delta$),

$$\begin{aligned} \hat{H}_{\text{car}} &= \frac{\hbar}{2}\Omega(\hat{\sigma}^+ e^{i\phi_c} + \hat{\sigma}^- e^{-i\phi_c}), \\ \hat{H}_{\text{bsb}} &= i\eta\frac{\hbar}{2}\Omega(\hat{\sigma}^+ \hat{a}^\dagger e^{i\phi_b} e^{-i\delta t} - \hat{\sigma}^- \hat{a} e^{-i\phi_b} e^{i\delta t}), \\ \hat{H}_{\text{rsb}} &= i\eta\frac{\hbar}{2}\Omega(\hat{\sigma}^+ \hat{a} e^{i\phi_r} e^{i\delta t} - \hat{\sigma}^- \hat{a}^\dagger e^{-i\phi_r} e^{-i\delta t}), \end{aligned} \quad (4)$$

where $\delta \ll \omega_m$. As shown in Fig. 2, the carrier transition $|0, n\rangle \leftrightarrow |1, n\rangle$ is driven with Rabi frequency Ω , while the blue ($|0, n\rangle \leftrightarrow |1, n+1\rangle$) and red sideband transitions ($|0, n\rangle \leftrightarrow |1, n-1\rangle$) are driven with the Rabi frequencies of $\eta\Omega\sqrt{n+1}$ and $\eta\Omega\sqrt{n}$, respectively.

For an ion-qubit coupled with a single vibrational mode by a near-resonant field, the qubit-state-dependent force can be achieved by combining the blue and red sideband transitions,

$$\begin{aligned} \hat{H}_{\text{SDF}} &= \hat{H}_{\text{rsb}} + \hat{H}_{\text{bsb}} \\ &= \eta\frac{\hbar}{2}\Omega(\hat{a}^\dagger e^{i\phi_m} e^{-i\delta t} + \hat{a}e^{-i\phi_m} e^{i\delta t})\hat{\sigma}^{\phi_S}, \end{aligned} \quad (5)$$

in which we have $\phi_S = (\phi_b + \phi_r - \pi)/2$, $\phi_m = (\phi_b - \phi_r)/2$, and $\hat{\sigma}^{\phi_S} = \hat{\sigma}^x \cos \phi_S + \hat{\sigma}^y \sin \phi_S$. It is clear that ϕ_S and ϕ_m correlate to the phase of qubit state and vibrational mode, respectively [17, 90].

For the sake of ubiquity, we can generalize the above Hamiltonian in the following way [17, 90],

$$\hat{H}_{\text{SDF}} = i\hbar(\gamma(t)\hat{a}^\dagger - \gamma^*(t)\hat{a})\hat{\sigma}^{\phi_S}, \quad (6)$$

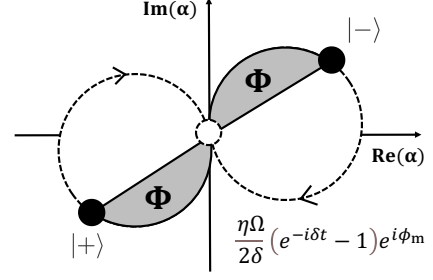


FIG. 3. The trajectory of motion is driven by the spin-dependent force in the phase space. The state $|+\rangle$ and $|-\rangle$ represent the two eigenstates of $\hat{\sigma}^{\phi_S}$ with eigenvalues $+1$ and -1 , respectively.

and the unitary evolution can be written as

$$\hat{U}(t) = \hat{D}(\alpha(t)\hat{\sigma}^{\phi_S}) \exp(i\Phi(t)), \quad (7)$$

where \hat{D} is the displacement operator, and $\Phi(t)$ is the geometric phase [17]. The expressions of $\gamma(t)$, $\alpha(t)$, and $\Phi(t)$ are expressed as the following way,

$$\begin{aligned} \gamma(t) &= -i\frac{\Omega}{2}\eta e^{-i\delta t} e^{i\phi_m}, \\ \alpha(t) &= \int_0^t \left(-i\frac{\Omega}{2}\eta e^{-i\delta t} e^{i\phi_m}\right) dt = \frac{\Omega\eta e^{i\phi_m}}{2\delta} (e^{-i\delta t} - 1), \\ \Phi(t) &= \text{Im} \left(\int_0^t \alpha(t')^* d\alpha(t') \right). \end{aligned} \quad (8)$$

When $\delta = 0$, the spin-dependent force can be simplified to the following expression,

$$\hat{H}_{\text{SDF}}^{\delta=0} = \eta\frac{\hbar}{2}\Omega(\hat{a}^\dagger e^{i\phi_m} + \hat{a}e^{-i\phi_m})\hat{\sigma}^{\phi_S}, \quad (9)$$

where the corresponding terms are $\gamma(t) = -i\Omega\eta e^{i\phi_m}/2$, $\alpha(t) = -i\Omega\eta e^{i\phi_m} t/2$, which results in no geometric phase as $\Phi(t) = 0$.

However, when the detuning $\delta \neq 0$, the evolution of α will go through a circular trajectory, as is drawn in Fig. 3. The left and right branches of this figure which circle in different directions corresponding to the positive and negative eigenstate of $\hat{\sigma}^{\phi_S}$, will generate the same geometric phases equal to the size of the encapsulated area. When the trajectories loop back to the origin, the motional states are disentangled from the spin states.

By far, we have illustrated a means of generating σ^{ϕ_S} -spin-dependent force, which directly leads to the MS gates. We note that the spin-dependent force can be realized in σ^z -basis as discussed in [15–17], which leads to the LS gates.

Laser gate

In ion trap systems, the two-qubit entangling gates can still be implemented via the coupling between the internal states and the collective vibrational modes. In this section, we mainly focus on using a single collective mode and later we will discuss the general situation with more-than one collective vibrational mode.

The trapped-ion entangling gates can be realized in various different ways with or without laser beams. Throughout the years, employing combinations of tunable lasers to implement multi-qubit gates has been the most prevalent and adhibited scenario, either for the hyperfine qubits or the optical qubits. The hyperfine qubits are typically incorporated with Raman transitions and the optical qubits are operated by applying direct transitions with narrow-linewidth.

The original entangling gate between two ion-qubits was proposed by Cirac and Zoller [1] and realized with a single qubit and two qubits [2, 3]. However, the CZ gate requires cooling to the ground state of the collective vibrational mode and the laser addressing on individual ions, which made it difficult to realize high-fidelity gates.

Different from the CZ gate scheme, the Mølmer-Sørensen (MS) gate [10–12] is independent with phonon number $|n\rangle$ of the vibrational mode of the interest, which is more experimentally favorable than the CZ gate scheme. For the MS gate scheme, a pair of trapped ions are illuminated with bichromatic laser fields simultaneously, and the ions will be driven by the state-dependent force to follow different motional trajectories depending on qubit states in the position-momentum phase space [12, 17]. In order to be an entangling operation, the internal states should be disentangled at the end of the gate with the accumulated geometric phase of $\pi/4$. The MS gate scheme was firstly demonstrated with $^9\text{Be}^+$ hyperfine qubits [13] in 2000. The MS gates have been popularly demonstrated in many ion-trap groups with up to the fidelity of 99.9 % [18, 91]. The effective gate-error rates of the two-qubit gates were also suppressed to $(0.96 \pm 0.10) \times 10^{-3}$ from 10^{-2} level of physical infidelity by using the error mitigation technique [92].

For MS gate, the spin-flip process is actualized by using a bichromatic laser whose central frequency corresponds to the single-flip resonance frequency, and the sideband frequency is slightly detuned from the vibrational mode, as Fig. 4 shows [93]. To simplify our discussion, only one axial mode will be included below. In this way, the Hamiltonian may be derived from directly extending Eq. (5) to a two-ion scenario [17],

$$\hat{H}_{\text{SDF}} = \sum_{j=1}^2 \eta_j \frac{\hbar\Omega}{2} (\hat{a}^\dagger e^{-i\delta t} e^{i\phi_{m,j}} + \hat{a} e^{i\delta t} e^{-i\phi_{m,j}}) \hat{\sigma}_j^{\phi_{s,j}}, \quad (10)$$

where η_j and $\phi_{m,j}$ represent the Lamb-Dicke parameter and the phase correlated to the vibrational mode of each

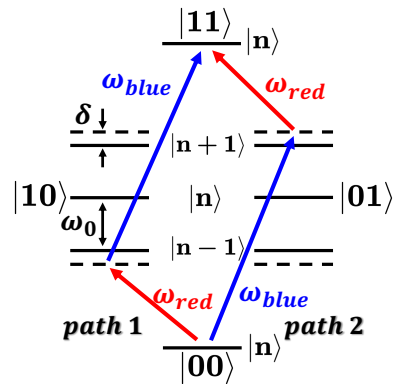


FIG. 4. The illustration of two typical paths for MS gate, which are driven by the bichromatic laser fields regardless of the phonon number $|n\rangle$, and the ω_0 and δ are the qubit frequency and laser detuning.

ion, respectively. Suppose we have $\phi_{s,1} = \phi_{s,2} = \phi_s$, then, the above Hamiltonian will lead to the following evolution operator,

$$\hat{U}(t) = \exp \left[\sum_{j=1}^2 (\alpha_j(t) a^\dagger - \alpha_j^*(t) a) \hat{\sigma}_j^{\phi_s} - i \frac{\theta(t)}{2} \hat{\sigma}_1^{\phi_s} \hat{\sigma}_2^{\phi_s} \right], \quad (11)$$

where

$$\alpha_j(t) = -i \frac{\eta_j \Omega}{2} \int_0^t e^{-i\delta t} e^{i\phi_{m,j}} dt = \frac{\Omega \eta_j e^{i\phi_{m,j}}}{2\delta} (e^{-i\delta t} - 1), \quad (12)$$

$$\theta(t) = \eta_1 \eta_2 \Omega^2 \left(\frac{t}{\delta} - \frac{\sin(\delta t)}{\delta^2} \right). \quad (13)$$

Viewing from phase space, the internal ion states will be fully disentangled with the vibrational mode after the phase trajectories $\alpha_j(t)$ of Eq. (12) are closed, and the first term of Eq. (11) disappears. At this time, $\theta(t)$ the geometric phase of the two-ion gate shown in Eq. (13) is obtained [12], and the evolution of MS interaction can be simplified to [94],

$$\hat{U}(\theta) = \exp \left(-i \frac{\theta}{2} \hat{\sigma}_1^{\phi_s} \hat{\sigma}_2^{\phi_s} \right). \quad (14)$$

Another typical two-qubit entangling gate scheme was proposed by Milburn in 2000 [15] and demonstrated with $^9\text{Be}^+$ hyperfine qubits [16], which is so-called LS gate. Similar to the MS gate scheme, the LS gate is also driven by the state-dependent force and generates the entangling interaction between ion qubits with the collective vibrational mode. However, the $|0\rangle \leftrightarrow |1\rangle$ states transition is not required during LS gate operation. LS gate is mainly achieved by applying two beams with a frequency difference close to a target vibration mode, which is coupled in the direction along the wavevector difference. In

the Lamb-Dicke regime and the rotating wave approximation, the interaction hamiltonian can be written as:

$$\hat{H}_I = \sum_{j=1,2} \sum_{s=0,1} \frac{\hbar\eta_j}{2} \Omega_s |s\rangle \langle s|_j \left[\hat{a} e^{i(\delta t - \phi_{m,j})} + \hat{a}^\dagger e^{-i(\delta t - \phi_{m,j})} \right]. \quad (15)$$

When we have $\Omega_0 = -\Omega_1 = \Omega$, we may transform the Hamiltonian into the following form:

$$\hat{H}_{\text{SDF}} = \sum_{j=1}^2 \eta_j \frac{\hbar\Omega}{2} (\hat{a}^\dagger e^{-i\delta t} e^{i\phi_{m,j}} + \hat{a} e^{i\delta t} e^{-i\phi_{m,j}}) \hat{\sigma}_j^z. \quad (16)$$

We can immediately discover that the above Hamiltonian of Eq. (16) is almost the same as the MS gate Hamiltonian of Eq. (10), except $\hat{\sigma}_j^{\phi_s}$ is replaced by $\hat{\sigma}_j^z$, which indicates the similarity of the MS gate and the LS gate. In this case, we may acquire the evolution operator in a form similar to Eq. (11),

$$\hat{U}(t) = \exp \left[\sum_{j=1}^2 (\alpha_j(t) a^\dagger - \alpha_j^*(t) a) \hat{\sigma}_j^z - i \frac{\theta}{2}(t) \hat{\sigma}_1^z \hat{\sigma}_2^z \right], \quad (17)$$

where the definition of $\alpha_j(t)$ and $\theta(t)$ directly follow Eqs. (12, 13). When the single qubit interaction terms vanish, we have,

$$\hat{U}(\theta) = \exp \left(-i \frac{\theta}{2} \hat{\sigma}_1^z \hat{\sigma}_2^z \right). \quad (18)$$

The imperfection of the LS gate comes from multiple sources, including higher-order terms beyond the Lamb-Dicke regime, laser-control errors, motional decoherence, unwanted mode coupling, scattering error, etc. This type of gate has been demonstrated on hyperfine qubits [16, 19] and optical qubits [20, 95]. Fast gate with fidelity of 99.8% in 1.6 μs has been achieved on $^{43}\text{Ca}^+$ hyperfine qubits [96]. Bell-State with infidelity of $6(3) \times 10^{-4}$ without subtraction of experimental errors has been directly measured with $^{40}\text{Ca}^+$ optical qubits [97].

The LS gate was considered to be impossible to implement with field-insensitive qubits [17]. However, it was proposed to realize the LS gates with field-insensitive qubits by using the laser detunings at the middle of trap frequencies [93, 98] or narrow line transitions [99]. These LS gates with clock states have been realized [100–102].

The MS and LS gates have also been applied to the multi-species atomic ions [103–110]. The Oxford group has achieved gate fidelity of 99.8 % between a $^{43}\text{Ca}^+$ hyperfine qubit and a $^{88}\text{Sr}^+$ Zeeman qubit [109].

Laser less gate

Microwave or RF field is used to implement high-fidelity single-qubit gates with convenient control capability of amplitude and phase. In order to couple qubit

and motion for multi-qubit gates, the strength of the field should vary significantly in the range of effective size of the ion, which is $z_0 \sim 10 \text{ nm}$. However, the gradient of the microwave or RF field is proportional to $1/\lambda \sim 1/100 \text{ mm}$, which is too small to drive the spin-motion interaction. In other words, the Lamb-Dicke parameter of the microwave field is around $\eta \sim 10^{-7}$, which produces negligible spin-motion coupling. A method to address this limitation is adding static magnetic fields with large gradients or using near-fields of the oscillating magnetic field, where the gradient is not limited by the wavelength of the field.

The static magnetic-field gradient used to realize spin-motion coupling was first proposed by Mintert and Wunderlich in 2001 [25]. When an ion interacts with a static magnetic-field gradient $\frac{\partial B_z}{\partial z}$ and a near-qubit-frequency microwave, the Hamiltonian can be expressed as below,

$$\hat{H} = \frac{1}{2} \hbar\omega_0 \hat{\sigma}^z + \hbar\omega_m \hat{a}^\dagger \hat{a} + \frac{1}{2} \mu_z (B_0 + \frac{\partial B_z}{\partial z} z) \hat{\sigma}^z + \hbar\Omega_\mu \hat{\sigma}^x \cos(\omega_\mu t), \quad (19)$$

where ω_0 is the qubit frequency, ω_m is the vibrational mode frequency, μ_z is the magnetic dipole moment, B_0 is the magnetic field at the equilibrium position of the ion, $\frac{\partial B_z}{\partial z}$ is the gradient of the magnetic field, z is the displacement around the equilibrium position, Ω_μ is the rabi frequency which quantifies the strength of dipole interaction, and ω_u is the microwave near-qubit-frequency. The displacement z can be changed to $z = z_0(\hat{a} + \hat{a}^\dagger)$, where $z_0 = \sqrt{\frac{\hbar}{2m\omega_m}}$, is the size of ground motional state. When applying the transform $\hat{H}' = e^{\hat{S}} \hat{H} e^{-\hat{S}}$, where $\hat{S} = \eta'(\hat{a}^\dagger - \hat{a}) \hat{\sigma}^z$, $\eta' = \frac{\mu_z z_0}{2\hbar\omega_m} \frac{\partial B_z}{\partial z}$, the interaction part of Eq.19 can be expressed as [25, 111]:

$$\hat{H}'_I = \frac{1}{2} \hbar\Omega_\mu (\hat{\sigma}^+ e^{\eta'(\hat{a}^\dagger - \hat{a})} + \hat{\sigma}^- e^{-\eta'(\hat{a}^\dagger - \hat{a})}) (e^{i\omega_\mu t} + e^{-i\omega_\mu t}). \quad (20)$$

As a consequence, the ion feels an effective Lamb-Dicke parameter η' , which means the qubit-motion coupling can be amplified by enlarging the gradient [112, 113]. From another perspective, if the gradient term is removed, the interaction term in Eq. 19 can only drive spin-flip with $\delta n = 0$. However, when introducing the gradient, the overlap between the motion states of $|0\rangle$ and $|1\rangle$ changed, which means the spin-flip with $\delta n \neq 0$ can be achieved, as shown in Fig. 5(a). The static magnetic-field gradient in experiments can be produced by permanent magnets [27, 28, 113] or wires with dc current [114–116]. Because of the spatially varied magnetic field, the resonance frequencies of ions are position-dependent, which provides a means to realize individual addressing by applying different microwave frequencies [112, 117]. The cross-talk of individual addressing by frequency selection was measured to be as low as 10^{-5} [118], where the cross-talk was quantified by the number of excitations in all

non-addressing qubits. The individual addressing methods were extended to the entangling gate operations, and nearest or non-nearest neighbor interactions of ions were demonstrated [27]. A shortcoming of the static magnetic-field gradient scheme is the necessity of using a magnetic-field sensitive qubit, where gate fidelity and coherence time can be seriously degraded by magnetic field fluctuation. A dressed state qubit with microwave, an effective clock qubit, was proposed and realized to show the coherence time is increased by two orders of magnitude to that of the bare magnetic-sensitive qubit [26]. The dressed qubits have been further developed and a two-qubit gate with the fidelity of 98.5 % and duration of 2.7 ms has been demonstrated [28, 64, 119–121].

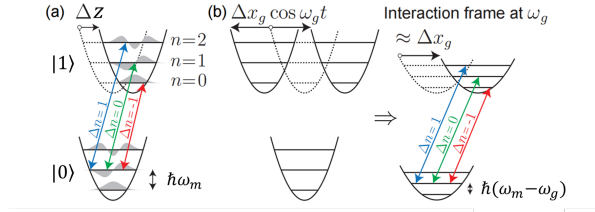


FIG. 5. Schematic description of a qubit coupled to a harmonic oscillator with a spin-dependent displacement from (a) a static magnetic field gradient or (b) an oscillating near-motion-frequency magnetic field gradient. Adapted from Ref. [31]

Oscillating near-qubit-frequency magnetic field gradient was proposed as an alternative method to couple qubit and motion [23]. Taking the gradient in the x -axis as an example, the interaction Hamiltonian can be written as:

$$\hat{H}_I = \mu_x \frac{\partial B}{\partial x} x_0 (\hat{a} + \hat{a}^\dagger) \hat{\sigma}_x \cos(\omega_g t), \quad (21)$$

where ω_g is the frequency near the qubit frequency ω_0 . When using interaction picture with $\hat{H}_0 = \frac{1}{2} \hbar \omega_0 \hat{\sigma}^z + \hbar \omega_m \hat{a}^\dagger \hat{a}$, \hat{H}_I can be rewritten as:

$$\hat{H}'_I = \hbar \hat{\sigma}_x \Omega_g \hat{a} e^{-i(\delta + \omega_m)t} + h.c., \quad (22)$$

where $\delta = \omega_g - \omega_0$, and $\Omega_g = \frac{\mu_x x_0}{2\hbar} \frac{\partial B}{\partial x}$. Therefore, the qubit-motion coupling can be achieved. In the experiment, microwave-based two-qubit $\hat{\sigma}_\phi \hat{\sigma}_\phi$ entangling gate was performed with the fidelity of 76(3) % [24] in 2011, whose near-qubit-frequency microwave gradient was created by the current in electrodes integrated into a microfabricated trap. Individual addressing was realized with spin-flip cross-talk errors on the order of 10^{-3} [122]. However, the fidelity of the two-qubit gate is greatly affected by residual microwave field and magnetic field fluctuation [123]. To alleviate these two limitations, the dynamical-decoupling method was applied to improve

the fidelity to 99.7 % with a gate time of 3.25 ms [29]. Another method to reduce the error from motional-mode frequency fluctuation by modulating the amplitude of the microwave was proved and realized to reach the mean fidelity of 99.7 % with the gate time of 2.938 ms [124]. The method of oscillating-magnetic field gradient was integrated into a surface trap and got the two-qubit fidelity of 98.2 % [125].

However, it is difficult to generate the gigahertz-frequency magnetic-field gradient for a hyperfine qubit. Recently, inspired by using running optical lattice to control the ion-motion [30], a new method to couple the spin and motion by combining near-motion-frequency oscillating magnetic field gradient with near-qubit-frequency microwave was proposed and applied to perform sideband cooling to its ground state [31]. In the scheme, the interaction Hamiltonian can be shown below:

$$\hat{H}_I = \hbar \Omega_g (\hat{a} + \hat{a}^\dagger) \hat{\sigma}_z \cos(\omega_g t) + \hbar \Omega_\mu \hat{\sigma}^x \cos(\omega_\mu t), \quad (23)$$

where $\Omega_g = \frac{\mu_z x_0}{2\hbar} \frac{\partial B_z}{\partial x}$, ω_g is the frequency near the motion frequency ω_m , ω_μ is the frequency near the qubit frequency ω_0 , and Ω_μ is the Rabi frequency of magnetic dipole interaction. Transforming to the interaction picture with respect to $\hat{H}_0 = \hbar \omega_g \hat{a}^\dagger \hat{a}$ and drop the fast term, the total Hamiltonian will change to:

$$\hat{H} = \frac{1}{2} \hbar \omega_0 \hat{\sigma}^z + \hbar (\omega_m - \omega_g) \hat{a}^\dagger \hat{a} \quad (24)$$

$$+ \frac{1}{2} \hbar \Omega_g \hat{\sigma}^z (\hat{a} + \hat{a}^\dagger) + \hbar \Omega_\mu \hat{\sigma}^x \cos(\omega_\mu t), \quad (25)$$

which is similar to the Hamiltonian in static magnetic field gradient method, except changing the ω_m to $\omega_m - \omega_g$ in Eq. (19) showed in Fig. 5(b). In the experiment, a robust gate to qubit frequency fluctuations and motional decoherence was proposed by using intrinsic dynamical decoupling [126]. The experimental realization of the gate produced a symmetric entangled state with near-perfect fidelity and antisymmetric with 99.77 % [32].

IV. DISCUSSION ABOUT THE CONTROL METHODS

Recently many modulation schemes have been developed for the entangling gate operations with trapped ions. The main purposes to include modulations in the gate can be categorized as the following three: (1) to make the gate robust against experimental imperfections, (2) to speed up the gate, and (3) to implement the gates in a single trap with multiple ions.

As discussed in the previous section, a perfect two-qubit entangling gate should satisfy two constraints at the end of the gate: (a) The trajectory in the phase space of the vibrational mode of an ion chain is closed. (b) The areas enclosed by the phase-space trajectory in the

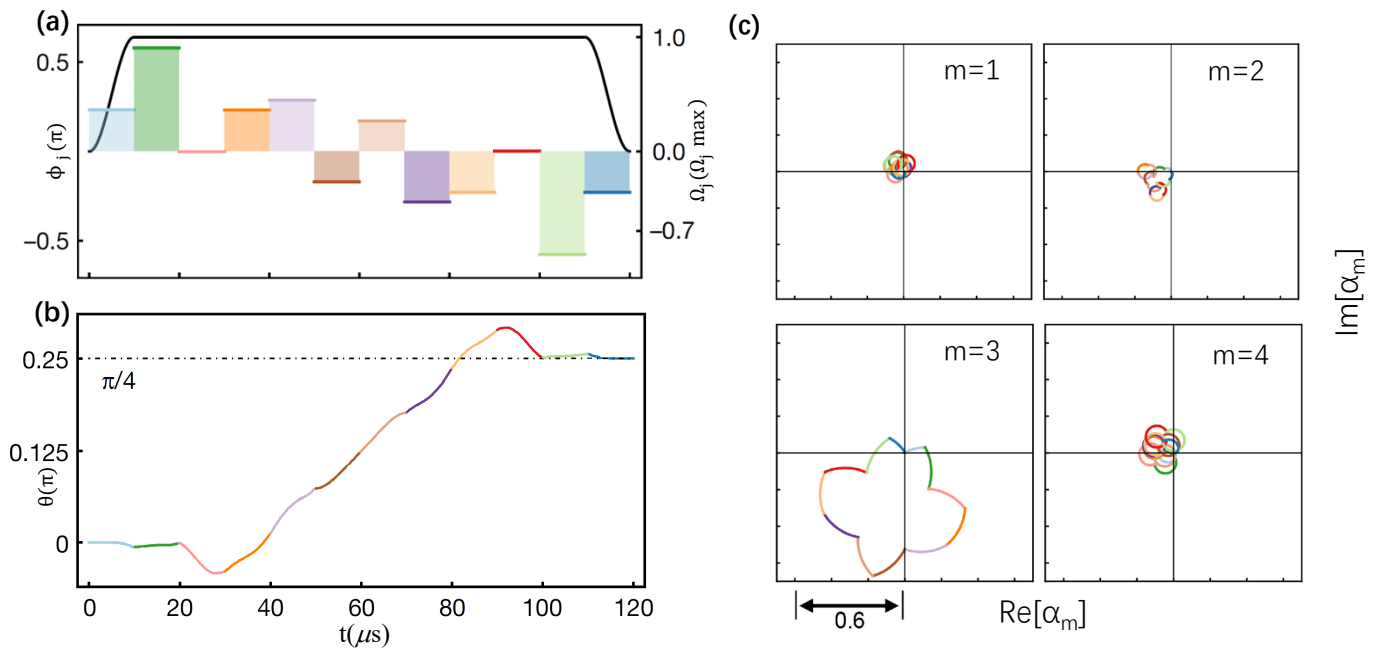


FIG. 6. Scheme for an entangling operation on the two ion-qubits in the middle of a four-ion chain. (a) The modulation scheme of the pulse sequence in motional phase ϕ_j and the amplitude, the Rabi frequency Ω_j , which are corresponding to the colored segments and the black solid curve respectively. (b) Accumulation in the geometric phase θ on the middle two ion-qubits. (c) Phase-space trajectories of four vibration modes. Modified from [49]

mode are $\theta = \pi/4$. However, due to the experimental imperfections such as frequency fluctuations of the driving field, timing error of the gate, and amplitude fluctuation, the trajectory of the vibrational mode can not be closed as designed and the accumulated geometric phase may not be exactly $\pi/4$, which decreases the fidelity of gates. The robustness of gates against imperfections can be improved by including modulations on the driving fields.

The duration of two-qubit gates can be shortened by increasing the amplitude of Rabi-frequency Ω in Eq. (10). If the strength of sideband transitions $\eta\Omega$ is comparable to the frequency difference of two vibrational modes, which are the center of mass (COM) and the stretch modes, we cannot use the single mode description discussed in the previous section. It is necessary to include the effects of both vibrational modes for the two-qubit gate operations. That is, the phase-space trajectories of both modes should be closed and the sum of the areas enclosed by the phase-space trajectories in both modes should be $\pi/4$ [38, 51, 127–130]. These requirements can be achieved by using the modulation methods and experimentally realized [88, 96].

One promising scheme to scale up the number of ions for quantum computation is to perform quantum gates on ion qubits confined in a long ion chain [34, 73, 82]. In the single-trap scheme, the transverse modes are more popularly used than axial modes. It is mainly due to the fact that better laser cooling can be achieved in transverse modes since the frequencies of transverse modes are

larger than those of axial modes in the linear chain with a large number of ions [35, 131]. However, the frequency spacings between the modes are getting smaller as the number of ions increases in the single linear trap, which makes it challenging to address only a single vibrational mode for the entangling gate. Similar to the fast gate, it is necessary to close all the trajectories of the modes and make the sum of the phase to be $\pi/4$ for target ions as shown in Fig. 6.

In order to achieve these goals, many different types of modulation such as amplitude [33–36, 38, 60, 93, 96, 124, 132], phase [32, 39–41, 133, 134], frequency modulation [42–44, 135, 136], and multi-frequency have been developed [45–48]. Here we briefly overview the developments of those modulations and discuss the multi-frequency modulation can provide a general method covering all the other modulation methods.

Amplitude

The amplitude modulation method is a scenario that changes the amplitude of the driving field, Ω in Eq. (10) from a constant to a time-dependent sequence during the gate operation.

Continuous-amplitude modulation scheme for two-qubit gates was proposed for robustness to the optical phase fluctuation of driving beams [93]. This scheme was applied to MS gates on optical qubits of $^{40}\text{Ca}^+$ ions

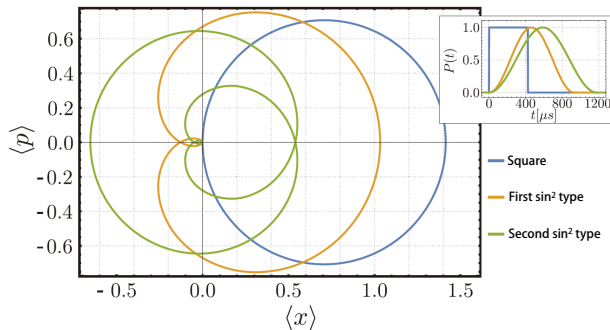


FIG. 7. The phase-space trajectories in the case of three amplitude-modulation schemes, which are square pulse (blue), first (orange) and second (green) \sin^2 type sequence shown in the inset [124].

with the duration of $50\mu s$ and the fidelity of 99.3% [60]. The amplitude-shaped pulses were also used to realize MS gates on the ions in the thermal state with average phonon number $\bar{n} = 20$, which showed the fidelity of 97.4 % in $25\mu s$ duration [132]. The continuous amplitude modulation is also applied to the MS gates by using a near-field microwave [124]. It was confirmed that this scheme is robust to frequency fluctuations of the vibrational modes. The gate was implemented with hyperfine qubits in $^9\text{Be}^+$ ions with 99.7 % fidelity [124]. The pulse timing and consequent phase space trajectory are as shown in Fig. 7.

The discrete amplitude modulation was proposed to realize two-qubit gates with multiple vibrational modes [33–35]. In the scheme, the laser field was divided into isochronous segments with different intensities to fulfill the constraints discussed above for ideal gates. This approach was implemented using hyperfine $^{171}\text{Yb}^+$ -ion qubits in a five-ion chain with gate time and fidelity of $190\mu s$ and 95%, respectively [36]. Another scheme of discrete amplitude modulation scheme was proposed to regard the duration and amplitude of each optical pulse as variables [38]. The optimal pulse sequence is considered to be insensitive to the optical phase of driving laser [38]. The above scenario was implemented in the hyperfine qubits of $^{43}\text{Ca}^+$ ions. The implemented two-bit gate has 99.8 % fidelity during $1.6\mu s$ [96]. Additionally, there are applications of the amplitude modulation gates, such as programmable quantum computer [37], and parallel entangling gates [50, 137].

Phase

The phase modulation (PM) method is to modulate the vibrational phases ϕ_j in Eq. (10) of the spin-dependent force during the gate operation. The PM has an advantage in experimental realization since it can be

more precisely controlled in the experiment than amplitude. The first PM was proposed to alternating the vibrational phases between 0 and π in the form of the Walsh functions for suppressing effects of a certain frequency and timing errors, which was realized with $^{171}\text{Yb}^+$ [133]. This scheme does not require optimizing the pulse sequence, but the duration of the gate increases as the higher orders of Walsh functions are used for enhanced robustness. The Walsh function method was also utilized in mixed-species [109] and $^{40}\text{Ca}^+$ [20] ions system. Similar to the Walsh function method, a phase modulation scheme based on the dynamical decoupling pulses technique has been proposed and implemented, which improved the robustness against dephasing noise of the qubit without much time overhead of the dynamical decoupling pulses [134].

A more flexible piecewise-constant PM scheme with continuous values of phases was proposed to implement two-qubit gates for both robustness and high fidelity with multiple vibrational modes [39]. This scheme was implemented in the hyperfine qubit of two $^{171}\text{Yb}^+$ ions, which demonstrated the robustness of this scheme to static or time-varying errors of laser amplitude and detuning. Their two-qubit achieves an average 99.4% fidelity in about $310\mu s$ [40].

We note that compared with amplitude modulation, it can change the orientation of the trajectory in phase space promptly, which is more proper to prevent the vibrational state of ions from being excited beyond the Lamb-Dicke regime and to implement a fast gate [51].

Frequency

The frequency modulation (FM) method is to modulate the laser frequency ω , which can be considered as μ above the Eq. (10). The FM was introduced for the robustness of the two-qubit gates with multiple vibrational modes [42]. The FM can be conceptually equivalent to the PM, but in the experimental realizations, wider ranges of frequencies are modulated, which cannot be simply converted to the PM. The FM is implemented by directly adjusting the frequency of the driving field through Acusto-Optic Modulator (AOM), but it will also change the deflection angle of the beam, causing errors in the offset of the beam focus point.

A continuous frequency-modulated laser was developed to minimize the residual spin-motion entanglement at the end of the two-qubit gate, making it robust to frequency error and achieving 98.3 % fidelity in experiments with 5 ions [42] as shown in Fig. 8.

With two individually addressed beams focused on the ion chain, discrete frequency modulation was applied to realize the two-qubit gate fidelity of 99.49 % in the 2-ion chain and 99.30 % fidelity in the 4-ion chain in $200\mu s$ [135]. Inspired by machine learning, the frequency

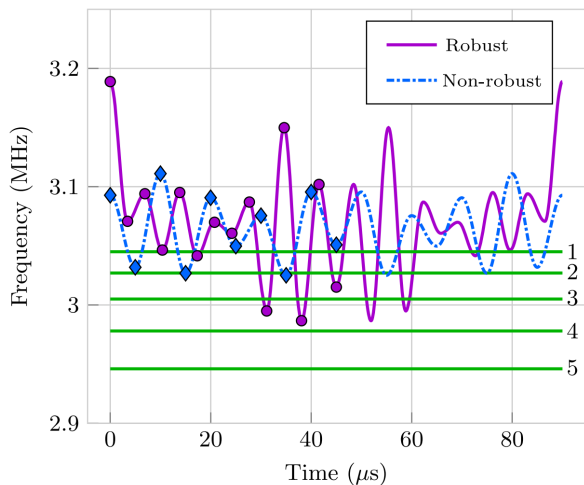


FIG. 8. Frequency modulation pulse for 2-qubit gate in 5-ion chain, the green lines are the mode frequencies. [42].

modulation gate was optimized by using a large sample set and mini-batches. The batch-optimized frequency-modulation gate reached the gate fidelity of 99.08 % in 120 μs [136].

Apart from the work with a single modulation, there are also progresses with two modulations, such as amplitude modulation plus frequency modulation [43, 44], amplitude modulation plus phase modulation [32, 41, 49].

Table I summarizes some representative works of recent experimental realization in two-qubit gates.

Multi-frequency Methods

The multi-frequency modulation method realizes the gate by simultaneously driving multiple-motional modes using the laser field of multiple frequencies with different amplitudes. It can provide the general and systematic control methods including all the effects of amplitude, phase, and frequency modulation.

The field for MS gates on j -th ion can be simplified as $\gamma_j(t) = \Omega_j e^{-i\mu t} e^{i\phi_{m,j}}$ as shown in Eq. (10). The amplitude, the phase, and the frequency of the field are Ω_j , $\phi_{m,j}$, and μ , respectively. We can generate an arbitrary waveform of the field with amplitude, phase, and frequency modulation by letting them the functions of time, which can be decomposed using Fourier expansion as

$$\gamma_j(t) = \sum_{n=-\infty}^{\infty} \Omega_{n,j} \exp(-in\omega t), \quad (26)$$

where $\Omega_{n,j}$ is a complex amplitude of n^{th} component of the frequency $n\omega$, and $\omega = \frac{2\pi}{\tau_g}$ with τ_g at the duration of the gate. This Fourier expansion can be seen as applying multi-frequency components. From the completeness of the Fourier series, we find the generality of the

multi-frequency method as an arbitrary modulation with amplitude, phase, and frequency.

The multi-frequency method was proposed to improve the gate performance and implement a global entangling gate [45]. It pointed out that the phase trajectories of a multi-tone gate are closer to closure under non-ideal conditions than single-tone gate [45]. These multi-frequency MS gates were realized with $^{171}\text{Yb}^+$ and $^{88}\text{Sr}^+$ ions in experiments and the robustness of the multi-frequency gates was experimentally verified against gate time error and frequency detuning drift [46, 47]. The multi-frequency method was further developed to include general constraints for robustness conditions to mitigate the effects of frequency drift, gate time offset, and carrier coupling to achieve a robust global entangling gate [48, 94]. In the next section, we will discuss the details of the multi-frequency methods for robustness, speed-up, and multi-qubit operations.

V. MULTI-FREQUENCY METHOD

In this section, first, we review the trapped-ion gates based on various state-dependant forces in detail, mainly for hyperfine qubits, and discuss the general framework of the multi-frequency methods. Finally, we consider the application of multi-frequency methods for fast and global entangling gates with and without individual addressing capability of the systems.

Various types of spin-dependent force

We first briefly recall the theory of the entangling gates based on the spin-dependent forces, covering both cases of the $\hat{\sigma}_\phi$ gate and the $\hat{\sigma}_z$ gate [17]. As mentioned above, transitions between qubit states can be driven by non-copropagating Raman lasers. Here we consider Raman couplings mediated by an excited electronic state $|e\rangle$, with laser configurations shown in Figs. 9 (a, b), and assume the net wave vector of the Raman process is parallel to the x -axis of the trap. To mitigate the spontaneous emission, the detuning Δ from the excited state is large, so the condition $\Delta \gg \omega_{\text{hf}}$ holds good in both cases. The interaction Hamiltonian between the ions and multiple lasers is written as follows (set Planck constant $\hbar = 1$),

$$\hat{H}(t) = \sum_i \sum_{\alpha} \sum_{s \in \{0,1\}} g_{\alpha,i,s} \cos(\mathbf{k}_\alpha \cdot \mathbf{r}_i - \omega_\alpha t - \phi_{\alpha,i}) \times (|e\rangle \langle s|_i + |s\rangle \langle e|_i), \quad (27)$$

with \mathbf{k}_α and ω_α being the wave vector and the frequency of the corresponding Raman laser. With the capability of single-ion addressing, it is possible to tune independently the single-photon Rabi frequency $g_{\alpha,i,s}$ and the phase $\phi_{\alpha,i}$, which provides enough freedom to construct

TABLE I. Summary of experimental realizations for two-qubit gates.

Modulation	Ions	Qubit	Control method	Ion number	Fidelity	Gate time	Year	Reference
Amplitude	$^{40}\text{Ca}^+$	Optical	Laser	Two	99.3%	$50\mu\text{s}$	2008	[60]
Amplitude	$^{171}\text{Yb}^+$	Hyperfine	Laser	Five	95.0%	$190\mu\text{s}$	2014	[36]
Amplitude	$^{43}\text{Ca}^+$	Hyperfine	Laser	Two	99.8%	$1.6\mu\text{s}$	2018	[96]
Amplitude	$^9\text{Be}^+$	Hyperfine	Microwave	Two	99.7%	$\sim 3000\mu\text{s}$	2019	[124]
Phase	$^{43}\text{Ca}^+, ^{88}\text{Sr}^+$	Hyperfine, Zeeman	Laser	Two	99.8%	$49.2\mu\text{s}$	2020	[109]
Phase	$^{171}\text{Yb}^+$	Hyperfine	Laser	Two	99.4%	$\sim 310\mu\text{s}$	2020	[40]
Phase	$^{25}\text{Mg}^+$	Hyperfine	Microwave	Two	$1_{-0.0017}^+$	$740\mu\text{s}$	2021	[32]
Phase	$^{40}\text{Ca}^+$	Optical	Laser	Two	99.94%	$35\mu\text{s}$	2021	[97]
Frequency	$^{171}\text{Yb}^+$	Hyperfine	Laser	Five	98.6%	$90\mu\text{s}$	2018	[42]
Frequency	$^{171}\text{Yb}^+$	Hyperfine	Laser	Four	99.30%	$200\mu\text{s}$	2020	[135]
None	$^{171}\text{Yb}^+$	Dress state	Microwave	Two	98.5%	2.7ms	2016	[28]
None	$^{43}\text{Ca}^+$	Hyperfine	Microwave	Two	99.7%	3.25ms	2016	[29]
None	$^{43}\text{Ca}^+$	Hyperfine	Laser	Two	99.9%	$\sim 100\mu\text{s}$	2016	[19]
None	$^9\text{Be}^+$	Hyperfine	Laser	Two	99.92%	$\sim 30\mu\text{s}$	2016	[18]
None	$^9\text{Be}^+$	Hyperfine	Microwave	Two	97.4%	$\sim 105\mu\text{s}$	2018	[138]
None	$^9\text{Be}^+$	Hyperfine	Microwave	Two	98.2%	$808\mu\text{s}$	2019	[125]
None	$^{171}\text{Yb}^+$	Hyperfine	Laser	Two	99.8%	$30\mu\text{s}$	2020	[139]

multi-qubit entangling operations including the global gate [140, 141].

For the case of the σ_ϕ -gate, the qubit states $|0\rangle$ and $|1\rangle$ can be encoded with hyperfine levels insensitive to the magnetic field, i.e. the clock states, which have the same single-photon Rabi frequencies, $g_{\alpha,i,0} = g_{\alpha,i,1} \equiv g_{\alpha,i}$. Transitions between the qubit levels can be induced by a monochromatic (subscripted by "A") and a bichromatic (subscripted by "Br" and "Bb") Raman lasers, as shown in Fig. 9 (a), with the frequency difference of the two Raman beams being around the hyperfine splitting ω_{hf} and the detuning of the stimulated Raman process to the carrier transition denoted by μ . If the frequency of Raman laser A is larger or smaller than both of the two frequencies in Raman laser B, the spin part of the effective laser-ion interaction after eliminating the excited state will depend on the optical phase difference between the Raman lasers. As a result, this type of entangling gate is called the phase-sensitive gate. (for example see Fig. 9 (c), where the frequencies of the Raman lasers can be set as $\omega_{Br} = \omega_A - \omega_{\text{hf}} + \mu$ and $\omega_{Bb} = \omega_A - \omega_{\text{hf}} - \mu$) After eliminating the excited state and introducing the Lamb-Dicke approximation, the effective laser-ion interaction Hamiltonian in the rotating frame is

$$\hat{H}_I(t) = \sum_m \omega_m \hat{a}_m^\dagger \hat{a}_m + \cos \mu t \sum_i \Omega_i \times \left[\hat{\sigma}_i^{\phi_i} + \sum_m \eta_{i,m} (\hat{a}_m^\dagger + \hat{a}_m) \hat{\sigma}_i^{(\phi_i - \frac{\pi}{2})} \right], \quad (28)$$

where the effective Rabi frequency and the spin phase are $\Omega_i = \frac{g_{A,i} g_{Br,i}}{2\Delta}$ and $\phi_i = \phi_{A,i} - \phi_{Br,i} - \delta k \bar{x}_i$, respectively, where we assume $g_{Br,i} = g_{Bb,i}$ and $\phi_{Br,i} = \phi_{Bb,i}$. Here the net-transferred wave vectors $\delta k \hat{\mathbf{e}}_x = \mathbf{k}_A - \mathbf{k}_{Br} = \mathbf{k}_A - \mathbf{k}_{Bb}$ are along the x -direction with the unit vector $\hat{\mathbf{e}}_x$ and \bar{x}_i

is the equilibrium position of the i -th ion. The site- and mode-resolved Lamb-Dicke parameters are $\eta_{i,m} = \eta_m b_{i,m}$ with $\eta_m = \delta k \sqrt{\frac{\hbar}{2M\omega_m}}$ and $b_{i,m}$ being the element of the matrix that diagonalizes the collective motion of the ion crystal.

On the other hand, if the frequency of Raman laser A is lying in between those of the Raman laser B, as shown in Fig. 9 (d), the effective ion-laser interaction Hamiltonian becomes,

$$\hat{H}_I(t) = \sum_m \omega_m \hat{a}_m^\dagger \hat{a}_m + \sum_i \Omega_i \left[\cos(\mu t - \phi_i) - \sin(\mu t - \phi_i) \sum_m \eta_{i,m} (\hat{a}_m^\dagger + \hat{a}_m) \right] \hat{\sigma}_i^x. \quad (29)$$

In this case, the spin part is independent of the phase difference of the Raman laser beams, thus leading to the phase-insensitive gate.

Besides the σ_ϕ -dependent force, it is also possible to induce σ_z -dependent force using magnetically sensitive hyperfine states, with the laser configuration shown in Fig. 9 (b), where there are both monochromatic lasers along the A and B optical paths. With the laser frequencies shown in Fig. 9 (e), i.e. $\omega_B = \omega_A - \mu$, the effective Hamiltonian becomes

$$\hat{H}_I(t) = \sum_m \omega_m \hat{a}_m^\dagger \hat{a}_m + \sum_i \Omega_i \left[\cos(\mu t - \phi_i) - \sin(\mu t - \phi_i) \sum_m \eta_{i,m} (\hat{a}_m^\dagger + \hat{a}_m) \right] \hat{\sigma}_i^z. \quad (30)$$

Note that in this case the effective Rabi frequency Ω_i depends on the differential AC-Stark effect, and thus this scheme only works for magnetically sensitive ion qubits. There is an alternative proposal for the light-shift or σ_z gate with clock-state qubits [93, 98, 99], which has been adopted by the Honeywell ion-trap group [101].

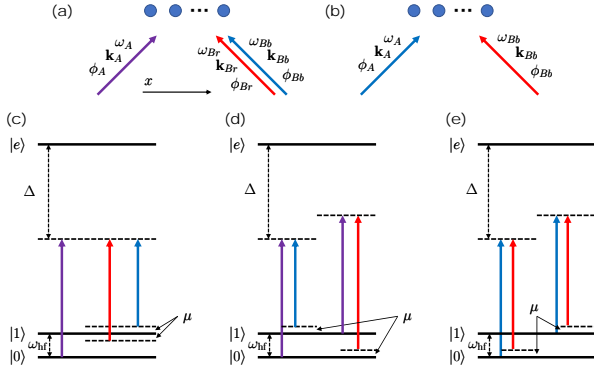


FIG. 9. Laser geometries. (a) Two non-copropagating Raman lasers shining on a trapped-ion chain. One of the two Raman lasers is monochromatic while the other is bichromatic. The detuning is around the qubit-state transition frequency. The direction of the net transferred wave vector is assumed to be along the axial direction. (b) The same as (a) with two monochromatic Raman laser beams. The detuning is around the frequencies of relevant motional modes. (c, d) Relevant energy levels and laser frequencies for the phase-sensitive gate (c) and the phase-insensitive gate. (e) The same as (c, d) for the $\hat{\sigma}^z$ gate.

General framework of multi-frequency method

For trapped-ion systems, the periods of the trapping potential provide a natural time scale for quantum operations. The characteristic time scales for the prementioned entangling gates involving a single motional mode are much longer than the trapping period. On the contrary, fast gates are operated on a time scale comparable with the trapping period. Intuitively, the laser intensities, as well as the Rabi frequencies, are large in order to exert enough influence on the trapped-ion system in such a short operation time, which results in non-negligible off-resonant carrier coupling and invalidation of the Lamb-Dicke approximation.

To derive fast gate schemes, we focus on the phase-insensitive $\hat{\sigma}^x$ gate and the light-shift $\hat{\sigma}^z$ gate. Despite the different laser configurations, the derivation can be unified by substituting $\hat{\sigma}_i^x$ in Eq. (29) and $\hat{\sigma}_i^z$ in Eq. (30) with $\hat{\sigma}_i^\alpha$ ($\alpha = x$, or z). The reason that we do not consider the phase-sensitive gate is that the effect of the carrier coupling cannot be canceled due to the $\pi/2$ phase difference between the carrier and the qubit part of the sideband terms. It is obvious from the effective Hamiltonians in Eqs. (29) and (30) that the detuning μ of the stimulated Raman process introduces an intensity modulation function in the spin-dependent force. In the slow region where the gate length is much longer than the trapping period, the detuning μ can be chosen to be close to a single motional mode, such that only this mode is excited and the others can be effectively eliminated in the dynamics. In this case, the monochromatic modulation

will suffice to disentangle the qubit state and the motional modes. In the fast regime, however, the frequency differences between μ and multiple motional modes are comparable with the Rabi frequency Ω , so multiple motional modes take part in the dynamics and need to be disentangled. To tackle this complicated situation, Refs. [45, 48, 51] proposed a multichromatic modulation scheme, which, compared to the prementioned monochromatic modulation scheme, introduces more controlling parameters to satisfy multiple constraints imposed by the requirements both to disentangle the motional modes and to apply effective spin-spin interactions.

In the Lamb-Dicke regime, the effective Hamiltonian with multichromatic modulation in the rotating frame is written as follows,

$$\hat{H}_I(t) = \sum_{i=1}^N \left[f_{\text{car},i}(t) + f_{\text{sdf},i}(t) \right] \hat{\sigma}_i^\alpha, \quad (31)$$

$$\times \sum_{m=1}^N \eta_{i,m} (\hat{a}_m e^{-i\omega_m t} + \hat{a}_m^\dagger e^{i\omega_m t})$$

with $\alpha \in \{x, z\}$ and the multichromatic modulation functions for the carrier and the spin-dependent force terms being

$$f_{\text{car},i}(t) = \Omega_i \sum_{k=1}^K r_{i,k} \cos(\nu_k t - \phi_{i,k}), \quad (32)$$

$$f_{\text{sdf},i}(t) = \Omega_i \sum_{k=1}^K r_{i,k} \sin(\nu_k t - \phi_{i,k}),$$

where Ω_i is the strength of the spin-dependent force and \vec{r} is a normalized dimensionless K -entry vector ($\|\vec{r}_i\|_2 = 1$) characterizing the distribution of laser power among different frequency components. The frequency components are determined by the gate duration τ , such that $\nu_k = 2k\pi/\tau$ ($k = 1, \dots, K$), which guarantees that the contribution of the carrier coupling always vanishes at the end of the dynamics. For the derivation to be succinct and clear, we set $\phi_{i,k} = 0$ for $\forall i$ and $\forall k$ irrespective of any position and frequency dependence that may exist in real systems. Later for the generality, we will consider gate schemes that are robust with respect to the overall fluctuation of the optical phases.

Using the Magnus expansion, we obtain the evolution operator $\hat{U}(t)$ as follows,

$$\hat{U}(t) = \exp \left[-i \sum_{i,m} \hat{B}_{i,m}(t) \hat{\sigma}_i^\alpha + i \sum_{i,j} \Theta_{i,j}(t) \hat{\sigma}_i^\alpha \hat{\sigma}_j^\alpha \right], \quad (33)$$

with $\hat{B}_{i,m}(t) = \beta_{i,m}^*(t) \hat{a}_m + \beta_{i,m}(t) \hat{a}_m^\dagger$, where $\beta_{i,m}(t)$ and $\Theta_{i,j}$ can be obtained as

$$\beta_{i,m}(t) = \eta_{i,m} \int_0^t f_{\text{sdf},i}(t') e^{i\omega_m t'} dt', \quad (34)$$

$$\Theta_{i,j}(t) = 2 \sum_m \eta_{i,m} \eta_{j,m} \int_0^t \int_0^{t'} f_{\text{sdf},i}(t'') \times f_{\text{sdf},j}(t''') \sin \omega_m(t' - t''') dt' dt'''. \quad (35)$$

To construct a target unitary operator with effective spin-spin interactions, i.e. $\hat{U}_{\text{tar}}(\tau) = \exp(-i \sum_{i < j} J_{i,j} \hat{\sigma}_i^\alpha \hat{\sigma}_j^\alpha)$, we obtain the following constraints to be satisfied at time $t = \tau$,

$$\beta_{i,m}(\tau) = 0, \quad \Theta_{i,j}(\tau) = J_{i,j}. \quad (36)$$

For an N -ion system, the number of constraints is $N^2 + \frac{N(N-1)}{2}$. Thus solutions exist as long as the variational modulation scheme provides more controlling parameters. Moreover, as variational modulation schemes always provide much more degrees of freedom, it is possible to search for optimized schemes with respect to realistic physical considerations. For example, we can require the maximum Rabi frequency to be as small as possible by optimizing a cost function $\mathcal{C}(\{\Omega_i, \vec{r}_i, \vec{\phi}_i\}) = \max_i |\Omega_i|$.

Framework of multi-frequency method with global control

In general trapped ion systems, individual control requires highly focused laser beams with the beam waist smaller than the spatial separation of ions. Thus it not only introduces complicated experimental instruments to generate and control the individual laser beams but also introduces extra errors in the manipulation procedure of the quantum system. For example, tiny movements in the ion position will lead to serious amplitude fluctuation in the Raman process, due to the steep profile of the highly-focused beams. Moreover, the residual electromagnetic field experienced by the neighboring ions also induces coherent crosstalk errors. Thus the entangling-gate schemes that ease the requirement for individual control always attract considerable attention.

Without individual control, the control parameters are reduced as $\Omega_i \equiv \Omega$, $\vec{r}_i \equiv \vec{r} = (r_1, \dots, r_K)$ and $\vec{\phi}_i \equiv \vec{\phi} = (\phi_1, \dots, \phi_K)$, with K being the number of frequency components. We further assume $\phi_k = \phi$ for simplicity. In this symmetric case, it is natural to define the collective spin operators $\hat{S}_m^\alpha = \sum_{i=1}^N b_{i,m} \hat{\sigma}_i^\alpha$ and the evolution operator in Eq. (33) is reduced to the following form,

$$\begin{aligned} \hat{U}(t) = \exp \left[-i \sum_{m=1}^N (\hat{a}_m A_m^*(t) + \text{h.c.}) \hat{S}_m^\alpha \right. \\ \left. + i \sum_{m=1}^N \Theta_m(t) \hat{S}_m^{\alpha 2} \right], \end{aligned} \quad (37)$$

with

$$A_m(t) = \eta_m \Omega \int_0^t f_{\text{sdf}}(t') e^{i\omega_m t'} dt', \quad (38)$$

$$\begin{aligned} \Theta_m(t) = \eta_m^2 \Omega^2 \int_0^t \int_0^{t'} f_{\text{sdf}}(t') f_{\text{sdf}}(t'') \\ \times \sin[\omega_m(t' - t'')] dt' dt''. \end{aligned} \quad (39)$$

For the all-to-all entangling gate, we required that at the end of the dynamics $t = \tau$ the following constraints are

satisfied,

$$\begin{aligned} A_m(\tau) = 0, \quad \forall m, \\ \Theta_1(\tau) = \pi/4, \quad \Theta_{m>1} = 0, \end{aligned} \quad (40)$$

where the first part is the aforementioned motion-spin disentangling condition. For target unitary that represents a general spin-spin interaction, $\hat{U}(\tau) = \exp(-\sum_{i < j} J_{i,j} \hat{\sigma}_i^\alpha \hat{\sigma}_j^\alpha)$, the effective interaction strength $J_{i,j}$ can be obtained as

$$J_{i,j} = 2 \sum_m \Theta_m(\tau) b_{i,m} b_{j,m}. \quad (41)$$

In other words, for a given set of $J_{i,j}$, gate schemes without individual control exist only when the linear-equation system in Eq. (41) has non-vanishing solutions.

Considerations for fast and robust global-entangling gate

When the gate length is comparable to the trapping period, the above gate scheme becomes sensitive to the fluctuation of the optical phases and the drift of the equilibrium ion positions. These effects result in an indefinite initial phase in the modulation function. Moreover, the required Rabi frequencies, which are proportional to the laser intensities, also increase as the gate length becomes shorter. Thus some of the motional modes are strongly driven during the evolution, and the Lamb-Dicke approximation may not always hold good. In other words, the higher-order terms of the Lamb-Dicke parameters cannot be neglected. In this case, a protocol obtained within the Lamb-Dicke approximation may suffer beyond-Lamb-Dicke error in experiment realization. Here we introduce two sets of constraints to guarantee the robustness of the resulting gate schemes with respect to the initial phase and higher-order terms.

To obtain robust gate schemes with respect to the drift of the initial phase, we notice that the modulation function in Eq. (32) can be decomposed as $f_{\text{sdf}}(t) \equiv f_s(t) \cos \phi + f_c(t) \sin \phi$, with

$$f_s(t) = \Omega \sum_{k=1}^K r_k \sin \nu_k t, \quad f_c(t) = \Omega \sum_{k=1}^K r_k \cos \nu_k t. \quad (42)$$

Note that before we obtain gate schemes for $\phi = 0$, where we consider linear constraints with $f_{\text{sdf}}(t) = f_s(t)$. Requiring the linear constraints $A_m(\tau) = 0$ be satisfied for arbitrary ϕ is equivalent to adding another set of linear constraints with $f_{\text{sdf}}(t) = f_c(t)$. Similarly, we decompose the quadratic constraints for $\Theta_m(\tau)$ into four sets of constraints. Figure 10 shows two-qubit gate schemes in a two-ion chain with the axial trapping frequency $\omega_z = 2\pi \times 1$ MHz. Without loss of generality, we assume the axial modes are driven and the gate duration is set to be $3.2 \mu\text{s}$. As expected, the robust gate scheme

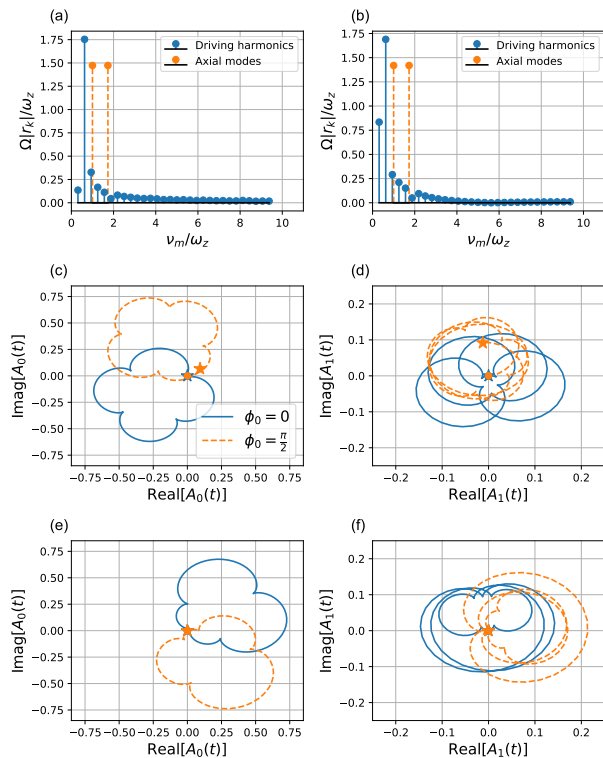


FIG. 10. Two-qubit entangling gate robust with respect to the initial phase drift. Here we assume the lasers are coupled to the axial- z modes, with the center-of-mass mode frequency ω_0 equal to the axial trapping frequency $\omega_z = 2\pi \times 1$ MHz. The gate duration is $\tau = 3.2 \mu\text{s}$ and $K = 30$ different driving harmonics with the frequency $\nu_k = 2k\pi/\tau$, $k = 1, 2, \dots, K$ are considered. (a) Driving amplitudes for the gate scheme without considering the robustness against the initial phase drift. The phase-space trajectories of the center-of-mass mode (c) and the stretch mode (d) are shown for different values of the initial phase ϕ_0 . (b, e, f) The same as (a, c, d) for a robust gate scheme considering the initial phase drift. In (c-f), the endpoints of the trajectories at the end of the gate operations are marked with stars. The gate schemes are obtained under the condition $\phi_0 = 0$, and only for the robust gate, the endpoints return to the origin for a drifted initial phase $\phi_0 = \pi/2$.

obtained in the above procedure is insensitive to the drift of the initial phase, as the endpoints of the trajectories of both motional modes come back to the origin at the end of the gate operation, as shown in Fig. 10 (e, f). Under the Lamb-Dicke approximation, the fidelity of the gate scheme without consideration of the initial phase drift decreases to 98.9% with $\phi_0 = \pi/2$, while the fidelity of the robust gate is always perfect irrespective of the initial phase. The cost of the robustness is, however, that the dimensionless magnitude of the Rabi frequency $|\Omega|/\omega_z$ increases from about 1.81 to 1.93. The amount of the increment becomes severe for gate schemes with shorter gate durations.

To suppress the beyond-Lamb-Dicke error, it is a nat-

ural way to first expand the effective Hamiltonian in Eq. (31) to the second order of the Lamb-Dicke parameters η_m . In this case, the evolution operator in Eq. (37) contains second-order terms, which depend linearly on the modulation function according to the Magnus expansion. As a result, there will be another set of linear constraints to be satisfied. Although errors induced by the second-order terms are suppressed, the resulting gate schemes always have much higher Rabi frequencies than the original gate scheme. As a result, these schemes only work well in the ultrafast regime, where the beyond-Lamb-Dicke errors are significant.

Comments on the individual control capability for multi-qubit gates

On the contrary, with the ability to individually address each qubit, the multi-qubit entangling gate scheme can be more flexible. For example, the global entangling gate scheme via individual phase modulation in Ref. [49] can be reduced to a similar gate involving fewer ion qubits by simply keeping the individual lasers shining on the selected ions and turning off the others. Intuitively, gate schemes with individual control are usually more efficient than those without individual control for entangling gates only involving a small part of the ions in a multi-qubit system. However, for a concrete target gate, the compromise between individual and global control needs to be considered seriously.

VI. CONCLUSION AND OUTLOOK

In this article, we review the quantum gates for trapped-ion quantum computation and quantum simulation. For the single qubit gates, it has been shown that the duration of the gates approach to picoseconds and the fidelities much higher than typical error correction requirements have been demonstrated with both microwaves and laser beams. For the two-qubit entangling gates, the main speed limit comes from the frequency of the vibrational modes, and the gates close to the limit have been demonstrated. The fidelities of the gates are limited by photon scatterings, heating and dephasing of the vibrational modes, dephasing of qubits, amplitude fluctuations of the laser fields, and so on. In principle, these errors can be further suppressed to below the level of 10^{-4} infidelity. Currently, one big challenge is to realize the gates with such high fidelity in a scalable way, either using ion shuttling or multiple ions in a single trap. One interesting quantum gate with trapped ions is the global gates that contain equivalently $\approx N^2/2$ gates in a single operation [49, 140, 141]. If a global gate can be realized at a speed close to the trap frequency, then the speed per two-qubit gates can be considered as the same factor

$\approx N^2/2$ of improvement.

Note- while preparing the manuscript, we learned that Ref. [142] reviewed the trapped-ion quantum gates, similar contents to this paper.

This work was supported by the innovation Program for Quantum Science and Technology under Grants No. 2021ZD0301602, and the National Natural Science Foundation of China under Grants No.92065205, and No.11974200.

* kimkihwan@mail.tsinghua.edu.cn

- [1] J. I. Cirac and P. Zoller, Quantum computations with cold trapped ions, *Phys. Rev. Lett.* **74**, 4091 (1995).
- [2] C. Monroe, D. M. Meekhof, B. E. King, W. M. Itano, and D. J. Wineland, Demonstration of a fundamental quantum logic gate, *Phys. Rev. Lett.* **75**, 4714 (1995).
- [3] F. Schmidt-Kaler, H. Häffner, M. Riebe, S. Gulde, G. Lancaster, T. Deuschle, C. Becher, C. F. Roos, J. Eschner, and R. Blatt, Realization of the cirac-zoller controlled-not quantum gate, *Nature* **422**, 408 (2003).
- [4] D. Leibfried, R. Blatt, C. Monroe, and D. Wineland, Quantum dynamics of single trapped ions, *Rev. Mod. Phys.* **75**, 281 (2003).
- [5] H. Häffner, C. F. Roos, and R. Blatt, Quantum computing with trapped ions, *Phys. Rep.* **469**, 155 (2008).
- [6] T. D. Ladd, F. Jelezko, R. Laflamme, Y. Nakamura, C. Monroe, and J. L. O'Brien, Quantum computers, *Nature* **464**, 45 (2010).
- [7] R. Blatt and C. F. Roos, Quantum simulations with trapped ions, *Nature Phys.* **8**, 277 (2012).
- [8] C. Monroe and J. Kim, Scaling the ion trap quantum processor, *Science* **339**, 1164 (2013).
- [9] C. Monroe, W. C. Campbell, L.-M. Duan, Z.-X. Gong, A. V. Gorshkov, P. Hess, R. Islam, K. Kim, N. M. Linke, G. Pagano, *et al.*, Programmable quantum simulations of spin systems with trapped ions, *Rev. Mod. Phys.* **93**, 025001 (2021).
- [10] A. Sørensen and K. Mølmer, Quantum computation with ions in thermal motion, *Phys. Rev. Lett.* **82**, 1971 (1999).
- [11] K. Mølmer and A. Sørensen, Multiparticle entanglement of hot trapped ions, *Phys. Rev. Lett.* **82**, 1835 (1999).
- [12] A. Sørensen and K. Mølmer, Entanglement and quantum computation with ions in thermal motion, *Phys. Rev. A* **62**, 022311 (2000).
- [13] C. A. Sackett, D. Kielpinski, B. E. King, C. Langer, V. Meyer, C. J. Myatt, M. Rowe, Q. Turchette, W. M. Itano, D. J. Wineland, *et al.*, Experimental entanglement of four particles, *Nature* **404**, 256 (2000).
- [14] E. Solano, R. L. de Matos Filho, and N. Zagury, Deterministic bell states and measurement of the motional state of two trapped ions, *Phys. Rev. A* **59**, R2539 (1999).
- [15] G. Milburn, S. Schneider, and D. James, Ion trap quantum computing with warm ions, *Fortschr. Phys.: Prog. Phys.* **48**, 801 (2000).
- [16] D. Leibfried, B. DeMarco, V. Meyer, D. Lucas, M. Barrett, J. Britton, W. M. Itano, B. Jelenković, C. Langer, T. Rosenband, *et al.*, Experimental demonstration of a robust, high-fidelity geometric two ion-qubit phase gate, *Nature* **422**, 412 (2003).
- [17] P. J. Lee, K.-A. Brickman, L. Deslauriers, P. C. Haljan, L.-M. Duan, and C. Monroe, Phase control of trapped ion quantum gates, *Journal of Optics B: Quantum and Semiclassical Optics* **7**, S371 (2005).
- [18] J. P. Gaebler, T. R. Tan, Y. Lin, Y. Wan, R. Bowler, A. C. Keith, S. Glancy, K. Coakley, E. Knill, D. Leibfried, *et al.*, High-fidelity universal gate set for be 9+ ion qubits, *Phys. Rev. Lett.* **117**, 060505 (2016).
- [19] C. Ballance, T. Harty, N. Linke, M. Sepiol, and D. Lucas, High-fidelity quantum logic gates using trapped-ion hyperfine qubits, *Phys. Rev. Lett.* **117**, 060504 (2016).
- [20] C. R. Clark, H. N. Tinkey, B. C. Sawyer, A. M. Meier, K. A. Burkhardt, C. M. Seck, C. M. Shappert, N. D. Guise, C. E. Volin, S. D. Fallek, *et al.*, High-fidelity bell-state preparation with ca+ 40 optical qubits, *Phys. Rev. Lett.* **127**, 130505 (2021).
- [21] D. Kielpinski, C. Monroe, and D. J. Wineland, Architecture for a large-scale ion-trap quantum computer, *Nature (London)* **417**, 709 (2002).
- [22] T. S. Metodi, D. D. Thaker, A. W. Cross, F. T. Chong, and I. L. Chuang, A quantum logic array microarchitecture: Scalable quantum data movement and computation, in *38th Annual IEEE/ACM International Symposium on Microarchitecture (MICRO'05)* (IEEE, 2005) pp. 12–pp.
- [23] C. Ospelkaus, C. E. Langer, J. M. Amini, K. R. Brown, D. Leibfried, and D. J. Wineland, Trapped-ion quantum logic gates based on oscillating magnetic fields, *Phys. Rev. Lett.* **101**, 090502 (2008).
- [24] C. Ospelkaus, U. Warring, Y. Colombe, K. Brown, J. Amini, D. Leibfried, and D. J. Wineland, Microwave quantum logic gates for trapped ions, *Nature* **476**, 181 (2011).
- [25] F. Mintert and C. Wunderlich, Ion-trap quantum logic using long-wavelength radiation, *Phys. Rev. Lett.* **87**, 257904 (2001).
- [26] N. Timoney, I. Baumgart, M. Johanning, A. Varón, M. B. Plenio, A. Retzker, and C. Wunderlich, Quantum gates and memory using microwave-dressed states, *Nature* **476**, 185 (2011).
- [27] A. Khromova, C. Piltz, B. Scharfenberger, T. Gloger, M. Johanning, A. Varón, and C. Wunderlich, Designer spin pseudomolecule implemented with trapped ions in a magnetic gradient, *Phys. Rev. Lett.* **108**, 220502 (2012).
- [28] S. Weidt, J. Randall, S. Webster, K. Lake, A. Webb, I. Cohen, T. Navickas, B. Lekitsch, A. Retzker, and W. Hensinger, Trapped-ion quantum logic with global radiation fields, *Phys. Rev. Lett.* **117**, 220501 (2016).
- [29] T. Harty, M. Sepiol, D. Allcock, C. Ballance, J. Tarlton, and D. Lucas, High-fidelity trapped-ion quantum logic using near-field microwaves, *Phys. Rev. Lett.* **117**, 140501 (2016).
- [30] S. Ding, H. Loh, R. Hablutzel, M. Gao, G. Maslennikov, and D. Matsukevich, Microwave control of trapped-ion motion assisted by a running optical lattice, *Phys. Rev. Lett.* **113**, 073002 (2014).
- [31] R. Srinivas, S. C. Burd, R. T. Sutherland, A. C. Wilson, D. J. Wineland, D. Leibfried, D. T. Allcock, and D. H. Slichter, Trapped-ion spin-motion coupling with microwaves and a near-motional oscillating magnetic field gradient, *Phys. Rev. Lett.* **122**, 163201 (2019).

- [32] R. Srinivas, S. Burd, H. Knaack, R. Sutherland, A. Kwiatkowski, S. Glancy, E. Knill, D. Wineland, D. Leibfried, A. C. Wilson, *et al.*, High-fidelity laser-free universal control of trapped ion qubits, *Nature* **597**, 209 (2021).
- [33] S.-L. Zhu, C. Monroe, and L.-M. Duan, Trapped ion quantum computation with transverse phonon modes, *Phys. Rev. Lett.* **97**, 050505 (2006).
- [34] S.-L. Zhu, C. Monroe, and L.-M. Duan, Arbitrary-speed quantum gates within large ion crystals through minimum control of laser beams, *EPL (Europhys. Lett.)* **73**, 485 (2006).
- [35] G.-D. Lin, S.-L. Zhu, R. Islam, K. Kim, M.-S. Chang, S. Korenblit, C. Monroe, and L.-M. Duan, Large-scale quantum computation in an anharmonic linear ion trap, *EPL (Europhys. Lett.)* **86**, 60004 (2009).
- [36] T. Choi, S. Debnath, T. Manning, C. Figgatt, Z.-X. Gong, L.-M. Duan, and C. Monroe, Optimal quantum control of multimode couplings between trapped ion qubits for scalable entanglement, *Phys. Rev. Lett.* **112**, 190502 (2014).
- [37] S. Debnath, N. M. Linke, C. Figgatt, K. A. Landsman, K. Wright, and C. Monroe, Demonstration of a small programmable quantum computer with atomic qubits, *Nature* **536**, 63 (2016).
- [38] A. M. Steane, G. Imreh, J. P. Home, and D. Leibfried, Pulsed force sequences for fast phase-insensitive quantum gates in trapped ions, *New J. Phys.* **16**, 053049 (2014).
- [39] T. J. Green and M. J. Biercuk, Phase-modulated decoupling and error suppression in qubit-oscillator systems, *Phys. Rev. Lett.* **114**, 120502 (2015).
- [40] A. R. Milne, C. L. Edmunds, C. Hempel, F. Roy, S. Mavadia, and M. J. Biercuk, Phase-modulated entangling gates robust to static and time-varying errors, *Phys. Rev. Applied* **13**, 024022 (2020).
- [41] C. D. Bentley, H. Ball, M. J. Biercuk, A. R. Carvalho, M. R. Hush, and H. J. Slatyer, Numeric optimization for configurable, parallel, error-robust entangling gates in large ion registers, *Advanced Quantum Technologies* **3**, 2000044 (2020).
- [42] P. H. Leung, K. A. Landsman, C. Figgatt, N. M. Linke, C. Monroe, and K. R. Brown, Robust 2-qubit gates in a linear ion crystal using a frequency-modulated driving force, *Phys. Rev. Lett.* **120**, 020501 (2018).
- [43] P. H. Leung and K. R. Brown, Entangling an arbitrary pair of qubits in a long ion crystal, *Phys. Rev. A* **98**, 032318 (2018).
- [44] K. A. Landsman, Y. Wu, P. H. Leung, D. Zhu, N. M. Linke, K. R. Brown, L. Duan, and C. Monroe, Two-qubit entangling gates within arbitrarily long chains of trapped ions, *Phys. Rev. A* **100**, 022332 (2019).
- [45] F. Haddadfarshi and F. Mintert, High fidelity quantum gates of trapped ions in the presence of motional heating, *New J. Phys.* **18**, 123007 (2016).
- [46] A. E. Webb, S. C. Webster, S. Collingbourne, D. Bretau, A. M. Lawrence, S. Weidt, F. Mintert, and W. K. Hensinger, Resilient entangling gates for trapped ions, *Phys. Rev. Lett.* **121**, 180501 (2018).
- [47] Y. Shapira, R. Shaniv, T. Manovitz, N. Akerman, and R. Ozeri, Robust entanglement gates for trapped-ion qubits, *Phys. Rev. Lett.* **121**, 180502 (2018).
- [48] Y. Shapira, R. Shaniv, T. Manovitz, N. Akerman, L. Peleg, L. Gazit, R. Ozeri, and A. Stern, Theory of robust multiqubit nonadiabatic gates for trapped ions, *Phys. Rev. A* **101**, 032330 (2020).
- [49] Y. Lu, S. Zhang, K. Zhang, W. Chen, Y. Shen, J. Zhang, J.-N. Zhang, and K. Kim, Global entangling gates on arbitrary ion qubits, *Nature* **572**, 363 (2019).
- [50] C. Figgatt, A. Ostrander, N. M. Linke, K. A. Landsman, D. Zhu, D. Maslov, and C. Monroe, Parallel entangling operations on a universal ion-trap quantum computer, *Nature* **572**, 368 (2019).
- [51] K. Wang, J.-F. Yu, P. Wang, C. Luan, J.-N. Zhang, and K. Kim, Fast multi-qubit global-entangling gates without individual addressing of trapped ions, *Quantum Sci. Technol.* **7**, 044005 (2022).
- [52] C. Langer, R. Ozeri, J. D. Jost, J. Chiaverini, B. Demarco, A. Ben-Kish, R. Blakestad, J. Britton, D. Hume, W. M. Itano, *et al.*, Long-lived qubit memory using atomic ions, *Phys. Rev. Lett.* **95**, 060502 (2005).
- [53] T. Harty, D. Allcock, C. J. Ballance, L. Guidoni, H. Janacek, N. Linke, D. Stacey, and D. Lucas, High-fidelity preparation, gates, memory, and readout of a trapped-ion quantum bit, *Phys. Rev. Lett.* **113**, 220501 (2014).
- [54] Y. Wang, M. Um, J. Zhang, S. An, M. Lyu, J.-N. Zhang, L.-M. Duan, D. Yum, and K. Kim, Single-qubit quantum memory exceeding ten-minute coherence time, *Nat. Photonics* **11**, 646 (2017).
- [55] P. Wang, C.-Y. Luan, M. Qiao, M. Um, J. Zhang, Y. Wang, X. Yuan, M. Gu, J. Zhang, and K. Kim, Single ion qubit with estimated coherence time exceeding one hour, *Nat. Commun.* **12**, 1 (2021).
- [56] A. Myerson, D. Szwed, S. Webster, D. Allcock, M. Curtis, G. Imreh, J. Sherman, D. Stacey, A. Steane, and D. Lucas, High-fidelity readout of trapped-ion qubits, *Phys. Rev. Lett.* **100**, 200502 (2008).
- [57] S. L. Todaro, V. Verma, K. C. McCormick, D. Allcock, R. Mirin, D. J. Wineland, S. W. Nam, A. C. Wilson, D. Leibfried, and D. Slichter, State readout of a trapped ion qubit using a trap-integrated superconducting photon detector, *Phys. Rev. Lett.* **126**, 010501 (2021).
- [58] T. Ruster, C. T. Schmiegelow, H. Kaufmann, C. Warschburger, F. Schmidt-Kaler, and U. G. Poschinger, A long-lived zeeman trapped-ion qubit, *Applied Phys. B* **122**, 1 (2016).
- [59] B. B. Blinov, D. Leibfried, C. Monroe, and D. J. Wineland, Quantum computing with trapped ion hyperfine qubits, *Quantum Information Processing* **3**, 45 (2004).
- [60] J. Benhelm, G. Kirchmair, C. F. Roos, and R. Blatt, Towards fault-tolerant quantum computing with trapped ions, *Nature Phys.* **4**, 463 (2008).
- [61] S. Olmschenk, K. C. Younge, D. L. Moehring, D. N. Matsukevich, P. Maunz, and C. Monroe, Manipulation and detection of a trapped yb^+ hyperfine qubit, *Phys. Rev. A* **76**, 052314 (2007).
- [62] A. Bermudez, X. Xu, R. Nigmatullin, J. O’Gorman, V. Negnevitsky, P. Schindler, T. Monz, U. Poschinger, C. Hempel, J. Home, *et al.*, Assessing the progress of trapped-ion processors towards fault-tolerant quantum computation, *Phys. Rev. X* **7**, 041061 (2017).
- [63] C. M. Shappert, J. T. Merrill, K. Brown, J. M. Amini, C. Volin, S. C. Doret, H. Hayden, C. Pai, and A. Harter, Spatially uniform single-qubit gate operations with near-field microwaves and composite pulse compensation, *New J. Phys.* **15**, 083053 (2013).

- [64] J. Randall, S. Weidt, E. Standing, K. Lake, S. Webster, D. Murgia, T. Navickas, K. Roth, and W. Hensinger, Efficient preparation and detection of microwave dressed-state qubits and qutrits with trapped ions, *Phys. Rev. A* **91**, 012322 (2015).
- [65] D. J. Wineland, R. E. Drullinger, and F. L. Walls, Radiation-pressure cooling of bound resonant absorbers, *Phys. Rev. Lett.* **40**, 1639 (1978).
- [66] W. Neuhauser, M. Hohenstatt, P. Toschek, and H. Dehmelt, Optical-sideband cooling of visible atom cloud confined in parabolic well, *Phys. Rev. Lett.* **41**, 233 (1978).
- [67] C. Monroe, D. Meekhof, B. King, S. R. Jefferts, W. M. Itano, D. J. Wineland, and P. Gould, Resolved-sideband raman cooling of a bound atom to the 3d zero-point energy, *Phys. Rev. Lett.* **75**, 4011 (1995).
- [68] C. Roos, T. Zeiger, H. Rohde, H. Nägerl, J. Eschner, D. Leibfried, F. Schmidt-Kaler, and R. Blatt, Quantum state engineering on an optical transition and decoherence in a paul trap, *Phys. Rev. Lett.* **83**, 4713 (1999).
- [69] J. Dalibard and C. Cohen-Tannoudji, Laser cooling below the doppler limit by polarization gradients: simple theoretical models, *JOSA B* **6**, 2023 (1989).
- [70] S. Ejtemaee and P. Haljan, 3d sisyphus cooling of trapped ions, *Phys. Rev. Lett.* **119**, 043001 (2017).
- [71] G. Morigi, J. Eschner, and C. H. Keitel, Ground state laser cooling using electromagnetically induced transparency, *Phys. Rev. Lett.* **85**, 4458 (2000).
- [72] C. Roos, D. Leibfried, A. Mundt, F. Schmidt-Kaler, J. Eschner, and R. Blatt, Experimental demonstration of ground state laser cooling with electromagnetically induced transparency, *Phys. Rev. Lett.* **85**, 5547 (2000).
- [73] Y. Lin, J. P. Gaebler, T. R. Tan, R. Bowler, J. D. Jost, D. Leibfried, and D. J. Wineland, Sympathetic electromagnetically-induced-transparency laser cooling of motional modes in an ion chain, *Phys. Rev. Lett.* **110**, 153002 (2013).
- [74] R. Lechner, C. Maier, C. Hempel, P. Jurcevic, B. P. Lanyon, T. Monz, M. Brownnutt, R. Blatt, and C. F. Roos, Electromagnetically-induced-transparency ground-state cooling of long ion strings, *Phys. Rev. A* **93**, 053401 (2016).
- [75] N. Scharnhorst, J. Cerrillo, J. Kramer, I. D. Leroux, J. B. Wübbena, A. Retzker, and P. O. Schmidt, Experimental and theoretical investigation of a multimode cooling scheme using multiple electromagnetically-induced-transparency resonances, *Phys. Rev. A* **98**, 023424 (2018).
- [76] E. Jordan, K. A. Gilmore, A. Shankar, A. Safavi-Naini, J. G. Bohnet, M. J. Holland, and J. J. Bollinger, Near ground-state cooling of two-dimensional trapped-ion crystals with more than 100 ions, *Phys. Rev. Lett.* **122**, 053603 (2019).
- [77] L. Feng, W. Tan, A. De, A. Menon, A. Chu, G. Pagano, and C. Monroe, Efficient ground-state cooling of large trapped-ion chains with an electromagnetically-induced-transparency tripod scheme, *Phys. Rev. Lett.* **125**, 053001 (2020).
- [78] M. Qiao, Y. Wang, Z. Cai, B. Du, P. Wang, C. Luan, W. Chen, H.-R. Noh, and K. Kim, Double-electromagnetically-induced-transparency ground-state cooling of stationary two-dimensional ion crystals, *Phys. Rev. Lett.* **126**, 023604 (2021).
- [79] D. Wineland, J. Bergquist, W. M. Itano, and R. Drullinger, Double-resonance and optical-pumping experiments on electromagnetically confined, laser-cooled ions, *Optics Lett.* **5**, 245 (1980).
- [80] J. C. Bergquist, R. G. Hulet, W. M. Itano, and D. J. Wineland, Observation of quantum jumps in a single atom, *Phys. Rev. Lett.* **57**, 1699 (1986).
- [81] W. Nagourney, J. Sandberg, and H. Dehmelt, Shelved optical electron amplifier: Observation of quantum jumps, *Phys. Rev. Lett.* **56**, 2797 (1986).
- [82] L. A. Zhukas, P. Svihra, A. Nomerotski, and B. B. Blinov, High-fidelity simultaneous detection of a trapped-ion qubit register, *Phys. Rev. A* **103**, 062614 (2021).
- [83] J. E. Christensen, D. Hucul, W. C. Campbell, and E. R. Hudson, High-fidelity manipulation of a qubit enabled by a manufactured nucleus, *npj Quantum Information* **6**, 1 (2020).
- [84] S. Crain, C. Cahall, G. Vrijsen, E. E. Wollman, M. D. Shaw, V. B. Verma, S. W. Nam, and J. Kim, High-speed low-crosstalk detection of a 171yb+ qubit using superconducting nanowire single photon detectors, *Comm. Phys.* **2**, 1 (2019).
- [85] W. Campbell, J. Mizrahi, Q. Quraishi, C. Senko, D. Hayes, D. Hucul, D. Matsukevich, P. Maunz, and C. Monroe, Ultrafast gates for single atomic qubits, *Phys. Rev. Lett.* **105**, 090502 (2010).
- [86] W.-X. Guo, Y.-K. Wu, Y.-Y. Huang, L. Feng, C.-X. Huang, H.-X. Yang, J.-Y. Ma, L. Yao, Z.-C. Zhou, and L.-M. Duan, Picosecond ion-qubit manipulation and spin-phonon entanglement with resonant laser pulses, *Phys. Rev. A* **106**, 022608 (2022).
- [87] J. Mizrahi, C. Senko, B. Neyenhuis, K. Johnson, W. Campbell, C. Conover, and C. Monroe, Ultrafast spin-motion entanglement and interferometry with a single atom, *Phys. Rev. Lett.* **110**, 203001 (2013).
- [88] J. Wong-Campos, S. Moses, K. Johnson, and C. Monroe, Demonstration of two-atom entanglement with ultrafast optical pulses, *Phys. Rev. Lett.* **119**, 230501 (2017).
- [89] R. Ozeri, W. M. Itano, R. Blakestad, J. Britton, J. Chiaverini, J. D. Jost, C. Langer, D. Leibfried, R. Reichle, S. Seidelin, *et al.*, Errors in trapped-ion quantum gates due to spontaneous photon scattering, *Phys. Rev. A* **75**, 042329 (2007).
- [90] P. C. Haljan, K.-A. Brickman, L. Deslauriers, P. J. Lee, and C. Monroe, Spin-dependent forces on trapped ions for phase-stable quantum gates and entangled states of spin and motion, *Phys. Rev. Lett.* **94**, 153602 (2005).
- [91] J. P. Home, D. Hanneke, J. D. Jost, J. M. Amini, D. Leibfried, and D. J. Wineland, Complete methods set for scalable ion trap quantum information processing, *Science* **325**, 1227 (2009).
- [92] S. Zhang, Y. Lu, K. Zhang, W. Chen, Y. Li, J.-N. Zhang, and K. Kim, Error-mitigated quantum gates exceeding phys. fidelities in a trapped-ion system, *Nat. Commun.* **11**, 1 (2020).
- [93] C. F. Roos, Ion trap quantum gates with amplitude-modulated laser beams, *New J. Phys.* **10**, 013002 (2008).
- [94] T. Manovitz, Y. Shapira, L. Gazit, N. Akerman, and R. Ozeri, Trapped-ion quantum computer with robust entangling gates and quantum coherent feedback, *PRX quantum* **3**, 010347 (2022).
- [95] B. C. Sawyer and K. R. Brown, Wavelength-insensitive, multispecies entangling gate for group-2 atomic ions, *Phys. Rev. A* **103**, 022427 (2021).

- [96] V. Schäfer, C. Ballance, K. Thirumalai, L. Stephenson, T. Ballance, A. Steane, and D. Lucas, Fast quantum logic gates with trapped-ion qubits, *Nature* **555**, 75 (2018).
- [97] C. R. Clark, H. N. Tinkey, B. C. Sawyer, A. M. Meier, K. A. Burkhardt, C. M. Seck, C. M. Shappert, N. D. Guise, C. E. Volin, S. D. Fallek, H. T. Hayden, W. G. Rellergert, and K. R. Brown, High-Fidelity Bell-State Preparation with $^{40}\text{Ca}^{+}$ Optical Qubits, *Phys. Rev. Lett.* **127**, 130505 (2021), arXiv:2105.05828 [physics, physics:quant-ph].
- [98] K. Kim, C. Roos, L. Aolita, H. Häffner, V. Nebendahl, and R. Blatt, Geometric phase gate on an optical transition for ion trap quantum computation, *Phys. Rev. A* **77**, 050303 (2008).
- [99] L. Aolita, K. Kim, J. Benhelm, C. F. Roos, and H. Häffner, High-fidelity ion-trap quantum computing with hyperfine clock states, *Phys. Rev. A* **76** (2007).
- [100] T. Monz, K. Kim, A. Villar, P. Schindler, M. Chwalla, M. Riebe, C. F. Roos, H. Häffner, W. Hänsel, M. Hennrich, *et al.*, Realization of universal ion-trap quantum computation with decoherence-free qubits, *Phys. Rev. Lett.* **103**, 200503 (2009).
- [101] C. Baldwin, B. Bjork, M. Foss-Feig, J. Gaebler, D. Hayes, M. Kokish, C. Langer, J. Sedlacek, D. Stack, and G. Vittorini, High-fidelity light-shift gate for clock-state qubits, *Phys. Rev. A* **103**, 012603 (2021).
- [102] D. J. Gorman, B. Hemmerling, E. Megidish, S. A. Moeller, P. Schindler, M. Sarovar, and H. Häffner, Engineering vibrationally assisted energy transfer in a trapped-ion quantum simulator, *Phys. Rev. X* **8**, 011038 (2018).
- [103] J. P. Home, Quantum science and metrology with mixed-species ion chains, *Adv. At. Mol. Opt. Phys.* **62**, 231 (2013).
- [104] T. R. Tan, J. P. Gaebler, Y. Lin, Y. Wan, R. Bowler, D. Leibfried, and D. J. Wineland, Multi-element logic gates for trapped-ion qubits, *Nature* **528**, 380 (2015).
- [105] C. Ballance, V. Schäfer, J. P. Home, D. Szwer, S. C. Webster, D. Allcock, N. M. Linke, T. Harty, D. Aude Craik, D. N. Stacey, *et al.*, Hybrid quantum logic and a test of bell's inequality using two different atomic isotopes, *Nature (London)* **528**, 384 (2015).
- [106] I. V. Inlek, C. Crocker, M. Lichtman, K. Sosnova, and C. Monroe, Multispecies trapped-ion node for quantum networking, *Phys. Rev. Lett.* **118**, 250502 (2017).
- [107] V. Negnevitsky, M. Marinelli, K. K. Mehta, H.-Y. Lo, C. Flühmann, and J. P. Home, Repeated multi-qubit readout and feedback with a mixed-species trapped-ion register, *Nature (London)* **563**, 527 (2018).
- [108] C. Bruzewicz, R. McConnell, J. Stuart, J. Sage, and J. Chiaverini, Dual-species, multi-qubit logic primitives for $\text{Ca}^{+}/\text{Sr}^{+}$ trapped-ion crystals, *npj Quantum Information* **5**, 1 (2019).
- [109] A. C. Hughes, V. M. Schäfer, K. Thirumalai, D. P. Nadlinger, S. R. Woodrow, D. M. Lucas, and C. J. Ballance, Benchmarking a high-fidelity mixed-species entangling gate, *Phys. Rev. Lett.* **125**, 080504 (2020), arXiv:2004.08162 [quant-ph].
- [110] P. Wang, J. Zhang, C.-Y. Luan, M. Um, Y. Wang, M. Qiao, T. Xie, J.-N. Zhang, A. Cabello, and K. Kim, Significant loophole-free test of kochen-specker contextuality using two species of atomic ions, *Science Advances* **8**, eabk1660 (2022).
- [111] S. Wölk and C. Wunderlich, Quantum dynamics of trapped ions in a dynamic field gradient using dressed states, *New J. Phys.* **19**, 083021 (2017).
- [112] M. Johanning, A. Braun, N. Timoney, V. Elman, W. Neuhauser, and C. Wunderlich, Individual addressing of trapped ions and coupling of motional and spin states using rf radiation, *Phys. Rev. Lett.* **102**, 073004 (2009).
- [113] K. Lake, S. Weidt, J. Randall, E. Standing, S. Webster, and W. Hensinger, Generation of spin-motion entanglement in a trapped ion using long-wavelength radiation, *Phys. Rev. A* **91**, 012319 (2015).
- [114] J. Chiaverini and W. Lybarger Jr, Laserless trapped-ion quantum simulations without spontaneous scattering using microtrap arrays, *Phys. Rev. A* **77**, 022324 (2008).
- [115] B. Lekitsch, S. Weidt, A. G. Fowler, K. Mølmer, S. J. Devitt, C. Wunderlich, and W. K. Hensinger, Blueprint for a microwave trapped ion quantum computer, *Sci. Adv.* **3**, e1601540 (2017).
- [116] J. Welzel, F. Stopp, and F. Schmidt-Kaler, Spin and motion dynamics with zigzag ion crystals in transverse magnetic gradients, *J. Phys. B: Atom. Mole. Opt. Phys.* **52**, 025301 (2018).
- [117] S. X. Wang, J. Labaziewicz, Y. Ge, R. Shewmon, and I. L. Chuang, Individual addressing of ions using magnetic field gradients in a surface-electrode ion trap, *Appl. Phys. Lett.* **94**, 094103 (2009).
- [118] C. Piltz, T. Sriarunothai, A. Varón, and C. Wunderlich, A trapped-ion-based quantum byte with 10- 5 next-neighbour cross-talk, *Nat. Commun.* **5**, 1 (2014).
- [119] S. Webster, S. Weidt, K. Lake, J. McLoughlin, and W. Hensinger, Simple manipulation of a microwave dressed-state ion qubit, *Phys. Rev. Lett.* **111**, 140501 (2013).
- [120] I. Cohen, S. Weidt, W. K. Hensinger, and A. Retzker, Multi-qubit gate with trapped ions for microwave and laser-based implementation, *New J. Phys.* **17**, 043008 (2015).
- [121] S. Weidt, J. Randall, S. Webster, E. Standing, A. Rodriguez, A. Webb, B. Lekitsch, and W. Hensinger, Ground-state cooling of a trapped ion using long-wavelength radiation, *Phys. Rev. Lett.* **115**, 013002 (2015).
- [122] U. Warring, C. Ospelkaus, Y. Colombe, R. Jördens, D. Leibfried, and D. J. Wineland, Individual-ion addressing with microwave field gradients, *Phys. Rev. Lett.* **110**, 173002 (2013).
- [123] U. Warring, C. Ospelkaus, Y. Colombe, K. R. Brown, J. Amini, M. Carsjens, D. Leibfried, and D. J. Wineland, Techniques for microwave near-field quantum control of trapped ions, *Phys. Rev. A* **87**, 013437 (2013).
- [124] G. Zarantonello, H. Hahn, J. Morgner, M. Schulte, A. Bautista-Salvador, R. Werner, K. Hammerer, and C. Ospelkaus, Robust and resource-efficient microwave near-field entangling $\text{be}^{+} 9$ gate, *Phys. Rev. Lett.* **123**, 260503 (2019).
- [125] H. Hahn, G. Zarantonello, M. Schulte, A. Bautista-Salvador, K. Hammerer, and C. Ospelkaus, Integrated 9be^{+} multi-qubit gate device for the ion-trap quantum computer, *npj Quantum Information* **5**, 1 (2019).
- [126] R. Sutherland, R. Srinivas, S. C. Burd, H. M. Knaack, A. C. Wilson, D. J. Wineland, D. Leibfried, D. Allcock,

- D. Slichter, and S. Libby, Laser-free trapped-ion entangling gates with simultaneous insensitivity to qubit and motional decoherence, *Phys. Rev. A* **101**, 042334 (2020).
- [127] J. J. García-Ripoll, P. Zoller, and J. I. Cirac, Speed optimized two-qubit gates with laser coherent control techniques for ion trap quantum computing, *Phys. Rev. Lett.* **91**, 157901 (2003).
- [128] L.-M. Duan, Scaling ion trap quantum computation through fast quantum gates, *Phys. Rev. Lett.* **93**, 100502 (2004).
- [129] R. L. Taylor, C. D. Bentley, J. S. Pedernales, L. Lamata, E. Solano, A. R. Carvalho, and J. J. Hope, A study on fast gates for large-scale quantum simulation with trapped ions, *Scientific Reports* **7**, 1 (2017).
- [130] E. Torrontegui, D. Heinrich, M. Hussain, R. Blatt, and J. J. García-Ripoll, Ultra-fast two-qubit ion gate using sequences of resonant pulses, *New J. Phys.* **22**, 103024 (2020).
- [131] K. Kim, M.-S. Chang, R. Islam, S. Korenblit, L.-M. Duan, and C. Monroe, Entanglement and tunable spin-spin couplings between trapped ions using multiple transverse modes, *Phys. Rev. Lett.* **103**, 120502 (2009).
- [132] G. Kirchmair, J. Benhelm, F. Zähringer, R. Gerritsma, C. F. Roos, and R. Blatt, Deterministic entanglement of ions in thermal states of motion, *New J. Phys.* **11**, 023002 (2009).
- [133] D. Hayes, S. M. Clark, S. Debnath, D. Hucul, I. V. Inlek, K. W. Lee, Q. Quraishi, and C. Monroe, Coherent error suppression in multiqubit entangling gates, *Phys. Rev. Lett.* **109**, 020503 (2012).
- [134] T. Manovitz, A. Rotem, R. Shaniv, I. Cohen, Y. Shapira, N. Akerman, A. Retzker, and R. Ozeri, Fast dynamical decoupling of the mølmer-sørensen entangling gate, *Phys. Rev. Lett.* **119**, 220505 (2017).
- [135] Y. Wang, S. Crain, C. Fang, B. Zhang, S. Huang, Q. Liang, P. H. Leung, K. R. Brown, and J. Kim, High-fidelity two-qubit gates using a microelectromechanical-system-based beam steering system for individual qubit addressing, *Phys. Rev. Lett.* **125**, 150505 (2020).
- [136] M. Kang, Q. Liang, B. Zhang, S. Huang, Y. Wang, C. Fang, J. Kim, and K. R. Brown, Batch optimization of frequency-modulated pulses for robust two-qubit gates in ion chains, *Phys. Rev. Applied* **16**, 024039 (2021).
- [137] N. Grzesiak, R. Blümel, K. Wright, K. M. Beck, N. C. Pimenti, M. Li, V. Chaplin, J. M. Amini, S. Debnath, J.-S. Chen, *et al.*, Efficient arbitrary simultaneously entangling gates on a trapped-ion quantum computer, *Nat. Commun.* **11**, 1 (2020).
- [138] T. R. Tan, J. P. Gaebler, R. Bowler, Y. Lin, J. D. Jost, D. Leibfried, and D. J. Wineland, Demonstration of a dressed-state phase gate for trapped ions, *Phys. Rev. Lett.* **110**, 263002 (2018), arXiv:1301.3786 [physics, physics:quant-ph].
- [139] C. Baldwin, B. Bjork, J. Gaebler, D. Hayes, and D. Stack, Subspace benchmarking high-fidelity entangling operations with trapped ions, *Phys. Rev. Research* **2**, 013317 (2020).
- [140] D. Leibfried, E. Knill, S. Seidelin, J. Britton, R. B. Blakestad, J. Chiaverini, D. B. Hume, W. M. Itano, J. D. Jost, C. Langer, *et al.*, Creation of a six-atom ‘schrödinger cat’ state, *Nature* **438**, 639 (2005).
- [141] T. Monz, P. Schindler, J. T. Barreiro, M. Chwalla, D. Nigg, W. A. Coish, M. Harlander, W. Hänsel, M. Hennrich, and R. Blatt, 14-qubit entanglement: Creation and coherence, *Phys. Rev. Lett.* **106**, 130506 (2011).
- [142] D. Yum and T. Choi, Progress of quantum entanglement in a trapped-ion based quantum computer, *Current Appl. Phys.* **41**, 163 (2022).